Validation of MUSES NH_3 observations from AIRS and CrIS against aircraft measurements from DISCOVER-AQ and a surface network in the Magic Valley

Karen E. Cady-Pereira[1], Xuehui Guo[2], Rui Wang[3], April B. Leytem[4], Chase Calkins[1], Elizabeth Berry[1], Kang Sun[5,6], Markus Müller[7], Armin Wisthaler[7], Vivienne H. Payne[8], Mark Shephard[9], Mark Zondlo[2], Valentin Kantchev[8,10]

[1] Atmospheric and Environmental Research Inc., Lexington, MA, USA
[2] Department of Environmental Sciences, University of Virginia, Charlottesville, VA, USA
[3] Department of Civil and Environmental Engineering, Princeton University, Princeton, NJ, USA
[4] United States Department of Agriculture-Agricultural Research Service, Kimberly, ID, USA
[5] Department of Civil, Structural and Environmental Engineering, University at Buffalo, Buffalo, New York, USA
[6] Research and Education in eNergy, Environment and Water (RENEW) Institute, University at Buffalo, Buffalo, New York, USA
[7] Institute for Ion Physics and Applied Physics, University of Innsbruck, Innsbruck, Austria
[8] Jet Propulsion Laboratory, California Institute of Technology, Pasadena, CA, USA
[9] Environment and Climate Change Canada, Toronto ON, Canada
[10] Instrument Software and Science Data Systems, Pasadena, CA, USA

Correspondence: Karen Cady-Pereira (kcadyper@aer.com)

Abstract.

Ammonia is a significant precursor of $PM_{2.5}$ particles and thus contributes to poor air quality in many regions. Furthermore, ammonia concentrations are rising due to the increase of large scale, intensive agricultural activities, which are often accompanied by greater use of fertilizers and concentrated animal feedlots. Ammonia is highly reactive, and thus highly variable and difficult to measure. Satellite based instruments, such as the Atmospheric Infrared Sounder (AIRS), and the Cross-Track Infrared Sounder (CrIS), have been shown to provide much greater temporal and spatial coverage of ammonia distribution and variability than is possible with in situ networks or aircraft campaigns, but the validation of these data is limited.

Here we evaluate MUSES ammonia retrievals from AIRS and CrIS against ammonia measurements from aircraft in the California Central Valley and in the Colorado Front Range. These are small datasets taken over high source regions under very different conditions: winter in California and summer in Colorado. Direct comparisons of the surface values of the retrieved profiles are biased very low in California (~40 ppbv) and slightly high in Colorado (~10 ppbv), but this bias appears to be primarily due to smoothing error, since applying the instrument operator

effectively reduces the bias to zero. We also compare three years of CrIS ammonia against an in situ network in the Magic Valley in Idaho We show that CrIS ammonia captures both the seasonal signal and the spatial variability in the Magic Valley, though it is biased low here also. In summary, this analysis substantially adds to the validation record but also points to the need for more validation under many different conditions and at higher altitudes.

1. Introduction

Ammonia (NH_3) is one of the most common forms of reactive nitrogen and the primary alkaline gas in the atmosphere. Intended and unintended releases of NH_3 into the environment over the last century have significantly altered the natural nitrogen cycle (Erisman et al., 2008), so that the current emission levels of ammonia are about four times higher than in previous centuries (Battye et al., 2017). The main sources of NH_3 are agricultural emissions, namely from livestock raising and fertilizer application (EDGAR-Emission Database for Global Atmospheric Research, 2014), which account for 80% of all emissions globally (Sutton et al., 2013; Behera et al., 2013). There are also some locally or seasonally significant sources NH_3, the most notable being biomass burning events, which can generate large amounts of NH_3 (Coheur et al., 2009; Whitburn et al., 2015, 2016). In urban areas automobiles with three-way catalytic converters (Sun et al., 2017) can be a major source of NH_3. Nowak et al. (2012) estimate that in the Los Angeles basin cars contribute as much as 50% of the total NH_3 emissions.

Ammonia is the dominant base in the atmosphere, and it plays a significant role in the formation of fine particulate matter ($PM_{2.5}$) (e.g., Aneja et al., 2003), which can penetrate deep into the lungs and severely impact the respiratory and circulatory systems (Pope et al., 2009). Paulot and Jacob (2014) have shown that the costs associated with the health impacts of NH_3 associated with food production for export in the US offset half the revenue from these exports. Long-term

exposure to ambient $PM_{2.5}$ is the leading environmental risk factor for premature mortality worldwide, leading to an estimated 2.5–3.4 million premature deaths annually (Cohen et al., 2017), 20% of which is estimated to stem from NH_3 emissions (Lelieveld et al., 2015). Ammonia emissions are regulated by the European Union (EU) and it is a criteria pollutant in Canada, but not yet in the US. However the EPA has published established regulations (http://www.nsrlaw.com/single-post/2017/06/19/EPA-NSR-Chief-Outlines-NSR-Changes-at-2017-AWMA-Conference) mandating that every state must set area specific significant emission rates (SERs) for NH_3. Since the emissions of NH_3 are a key factor in the formation of $PM_{2.5}$, reducing emissions can be an effective path to reduce air pollution (Liu et al., 2021).

Given the rapid growth of industrial-scale agriculture (e.g., increase in egg, milk and meat consumption), especially in Asia (e.g., Xu et al., 2016), NH_3 emissions are projected to increase greatly over the next few decades in many parts of the world. The reduction of NO_x emissions due to more stringent controls will reduce the contribution of NO_x to the deposition of reactive nitrogen, but Paulot et al. (2013) suggest that an increase in NH_3 emissions will likely compensate for this reduction. NH_3 and its derivatives are also quickly deposited in the ecosystems, increasing their eutrophication and reducing biodiversity (Erisman et al., 2008). There is thus growing recognition that NH_3 is an important pollutant, and that it will likely play a greater role in air quality and ecosystem health over the next decades, due to both the essential role NH_3 plays in feeding the world's population, and to the fact that the atmospheric emission potential of NH_3 is directly linked to increasing temperatures (Skjøth et al., 2013; Sutton et al., 2013). However, in situ measurements remain a challenge. NH_3 is easy to detect, but it is hard to measure accurately, especially for concentrations below 10 ppbv (von Bobrutzki et al., 2010).T here are many in situ techniques used to detect atmospheric NH_3 with varying time resolution

and precision, but the main issue affecting precision is the inlet rather than the instrument. NH_3 is sticky, and so it is challenging to get it into a given instrument quantitatively and quickly (Roscioli et al., 2016), (Pollack et al., 2019). This feature is critical for characterizing the abundance of NH_3 in the background atmosphere, for making measurements of NH_3 fluxes, and deploying instruments on aircraft. New open-path sensors avoid this issue, but they cannot be deployed in many situations (e.g., Berkhout et al., 2017, Miller et al., 2014). Consequently, the emissions of NH_3 outside of a limited set of well-instrumented locations remain poorly constrained, reducing the accuracy with which models can represent concentrations and variability. The high spatial and temporal variability of NH_3 (surface values can range from less than 0.1 to 200 ppbv or more) exacerbates the lack of continuous, spatially well sampled data over extensive regions. This also contributes to bottom-up inventories often underestimating emissions due to scaling difficulties (Nowak et al., 2012).

Satellite data, even though they come with their own uncertainties, provide by virtue of their spatial and temporal density, another option for quantifying these emissions. Currently there are multiple NH_3 datasets, with varying data record lengths and spatial coverage, obtained from the following instruments: the three Infrared Atmospheric Sounding Interferometer (IASI) instruments flying in a 9:30 am orbit, the Greenhouse Gases Observing Satellite (GOSAT) in a 1:30 pm orbit, along with the Tropospheric Emission Spectrometer (TES), the Atmospheric Infrared Sounder (AIRS), and the three Cross-Track Infrared Sounder (CrIS) instruments, all flying in a 1:30 pm orbit. The data obtained from these instruments has had numerous applications. Multiple papers (Van Damme et al., 2015a; Shephard et al., 2011; Shephard and Cady-Pereira, 2015; Warner et al.; 2016; Shephard et al., 2020, Wang et al., 2021) have shown that NH_3 measurements from infrared sensors capture NH_3 hotspots, such as the Indo-Gangetic

plain, eastern China and the American Midwest, as well as the expected regional seasonal variability and fire activity. Warner et al. (2017) used retrievals from AIRS to show definite positive trends in NH_3 concentrations over the US, the EU and China, which the authors ascribe to declines in SO_2 and NO_2 emissions in all three regions due to more stringent controls. Van Damme et al. (2018) used nearly a decade of IASI (ANNI-NH3-v2.1R-I) data to show that the emissions listed in the EDGAR (EDGAR, 2016) inventory for large source regions were wrong by as much as a factor of three; furthermore, emissions from smaller sources were often underestimated by an order of magnitude. Dammers et al. (2019) found similar results using CrIS (CFPR-v1.0) and IASI (ANNI-v2.2) NH_3 data. Zhu et al. (2013) have demonstrated that Tropospheric Emission Spectrometer (TES) NH_3 data over North America in the 2006–2009 period, though relatively sparse, could be used in an inverse modeling framework to constrain emissions sufficiently to improve agreement between GEOS-Chem output and surface measurements from the National Atmospheric Deposition Program (NADP) Ammonia Monitoring Network (AMoN) network (https://nadp.slh.wisc.edu/networks/ammonia-monitoring-network/). Using NH_3 measurements from CrIS (MUSES) and NO_2 measurements from TROPOMI, Cao et al. (2022) demonstrated that NH_3 emissions decreased substantially over downtown Los Angeles during the 2019 March COVID-19 lockdown; this result is in agreement with the conclusion from Nowak et al. (2012) that in urban areas traffic can be a major source of NH_3 and consequently greatly increase exposure to $PM_{2.5}$.

Yet in spite of the increasing use of NH_3 data from space-based instruments, validation of these data remains rather limited. Sun et al. (2015) compared a small set of NH_3 total columns from the TES instrument against columns derived from surface and aircraft measurements during the NASA Deriving Information on Surface conditions from Column and Vertically Resolved

Observations Relevant to Air Quality (DISCOVER-AQ) California 2013 campaign, and found small differences (less than 6%) and high correlation (R=0.82); however, note that TES, which is no longer operational, had much higher spectral resolution (0.06 cm^{-1}) and thus greater sensitivity to surface NH_3 and less interference from water vapor than the infrared sensors (AIRS, CrIS, IASI) currently providing data for NH_3 retrievals. Shephard et al. (2015) compared TES profiles against aircraft measurements taken during the 2013 Joint Canada–Alberta Implementation Plan for Oil Sands Monitoring (JOSM) campaign and showed that the TES profiles were unbiased. Warner et al. (2016) compared four NH_3 retrievals from AIRS against aircraft profiles obtained during DISCOVER-AQ California and found good qualitative agreement. Dammers et al. (2017) compared 218 IASI (IASI-LUT and IASI-NN) and CrIS (CFPR-v1.0) total columns and CrIS profiles against corresponding data from ground based Fourier Transform Infrared (FTIR) observations at seven FTIR sites in the Network for the Detection of Atmospheric Composition Change (NDACC): the FTIR and CrIS total columns from the combined data were well correlated (R=0.77) and mainly unbiased. Correlations at the individual sites ranged from 0.28 (Mexico City) to 0.86 (Bremen).

Van Damme et al. (2015b) carried out what is likely the most extensive evaluation of NH_3 measured from space, comparing IASI (IASI-LUT) NH_3 against data from six different monitoring networks in North America, Europe, Africa and China and from the California Research at the Nexus of Air Quality and Climate Change (CalNex) campaign in California. Most of the data from the surface networks were provided on bi-weekly or monthly scales: when IASI columns were converted to surface concentrations and averaged over the corresponding time period, they showed qualitative agreement in space and time with the surface data: the correlations in general were not high, though still significant (R=0.25 to 0.49). Recently Guo et

al. (2021) (hereafter Guo2021) compared NH_3 columns from IASI (ANNI-v3) with integrated profiles obtained from aircraft data during the Colorado 2014 DISCOVER-AQ campaign: the IASI columns were unbiased and significantly correlated (R=0.57). Guo2021 do point out that the instruments currently used to measure NH_3 from aircraft have large uncertainties due to limited accuracy and slow response to changing NH_3 concentrations.

To a varying degree all the studies above cite the same factors that complicate the validation of satellite NH_3 products:

- Different measurement time scales (weeks or days vs instantaneous), especially for surface networks
- High in situ instrument noise
- Validation results are strongly influenced by local atmospheric conditions and the vertical distribution of NH_3, which highlights the need for further validation campaigns under diverse conditions
- Sub-pixel inhomogeneity due to the high spatial-temporal variability of NH_3 driven by its short lifetime; thus the point data from an in situ instrument will only be partially correlated with the pixel scale data obtained from a satellite instrument

Our objective is to add to the validation record at the single pixel scale with retrievals from L1B radiances from both the AIRS and CrIS instruments. The retrieved profiles here are obtained with the MUlti-SpEctra, MUlti-SpEcies, MUlti-Sensors (MUSES) (Fu et al., 2013, 2016, 2018) algorithm, which provides profiles, total columns and uncertainty estimates, all of which can also be evaluated against in situ data. AIRS and CrIS NH_3 will be compared against PTR-MS data from the P-3B aircraft flown during DISCOVER-AQ campaigns in California and Colorado. Warner et al. (2016) also compared AIRS with DISCOVER-AQ, but their retrievals used cloud cleared radiances and extended over nine AIRS pixels (~45 km footprints at nadir). Using single

pixel radiances provides several advantages over "cloud cleared radiances": the propagation of uncertainties from the radiances is simpler (see section 2.2) and the retrieved information is obtained on smaller spatial scales, which is important for NH_3 (see section 5). This will be the first comparison of single pixel NH_3 profiles from either AIRS or CrIS against aircraft data. Aircraft campaigns are valuable in that they profile the vertical distribution of NH_3, allowing us to evaluate the performance of retrieval algorithms and to provide models with more realistic profiles; however they are by nature limited in their temporal coverage. In order to test the capability of MUSES NH_3 to capture temporal and spatial variability over an extended period, surface level CrIS NH_3 concentrations will also be evaluated against three years of data from a small monitoring network in the Magic Valley in Idaho. Section 2 will briefly review the NH_3 retrieval algorithm, section 3 will give an overview of the instruments, section 4 will present the analysis of the DISCOVER-AQ data and section 5 will follow with the analysis of the Magic Valley data; finally, section 6 will summarize our conclusions and discuss future work.

2. MUSES NH_3 Retrieval Algorithm and Data

2.1 MUSES Algorithm

The first nadir retrievals of NH_3, obtained using a prototype retrieval with data from the TES instrument (Beer et al., 2008), exploited the NH_3 ν_2 vibrational band between 960 and 970 cm^{-1} to demonstrate that TES could measure the variability in NH_3 along a transect in China. Shephard et al. (2011) implemented a full optimal estimation (OE) approach (Rodgers, 2000), which sought to reduce the difference between the measured CrIS radiances in ν_2 band and the calculated radiances from a radiative transfer model (Moncet et al., 2008). Before the OE algorithm was run an a priori profile was chosen from one of three possible profiles (Figure S1),

representing background, moderate and enhanced NH_3 concentrations. These profiles were derived by binning global distributions of NH_3 (Shephard et al., 2011) from the chemical transport model GEOS-Chem (Zhu et al., 2013). The profile is selected by applying an online/offline brightness temperature (BT) difference test centered around the 967 cm^{-1} line. The OE algorithm is then run as a refinement step, in which the a priori and the initial guess profiles are identical except for the background profile, for which the moderate profile is chosen as the initial guess, in order to provide Jacobians with some sensitivity.

The algorithm developed for the TES NH_3 retrievals has since been adapted with minor changes for CrIS (Shephard and Cady-Pereira, 2015; Shephard et al., 2020) and AIRS (this paper). The spectral retrieval window and the frequencies for the online/offline BT test were slightly modified for the CrIS and AIRS spectral resolutions, and a preliminary retrieval step to adjust the surface temperature and emissivity was introduced. This algorithm forms the core of the NH_3 component of the MUSES software used here and also of the CrIS Fast Physical Retrieval (CFPR) code, whose product has been used in a number of previous studies (e.g., Shephard and Cady-Pereira, 2015; Shephard et al., 2020; Dammers et al. (2017); Cao et al. (2022), Marais et al. (2021)). The two products have much in common (the same spectral microwindows, a priori selection, constraint matrices and forward model), but obtain temperature and water profiles and surface properties from different sources and use different software to carry out the optimal estimation (Table S2). Preliminary comparisons have shown good agreement on average between the two algorithms (Figure S2), but a full comparison is beyond the scope of this paper, as the objective here is the validation of the MUSES AIRS and CrIS NH_3 retrievals.

The MUSES algorithm is an end-to-end optimal estimation process that provides a complete characterization of the parameters involved in the radiative transfer processes in the infrared

region, using a multi-step approach. Before the NH_3 retrieval step is reached, the atmosphere has been well characterized by the previous retrieval steps: temperature and water vapor profiles, surface properties and cloud absorption are thus known and can be accounted for in the NH_3 retrieval, significantly reducing errors from radiatively interfering species. Other species, such as carbon monoxide and ozone, are also retrieved in separate steps. This ensures that the atmospheric state is derived using the same forward model and radiance data that are used in the NH3 retrieval, reducing possible sources of error. Since cloud optical depth is retrieved, cloud clearing algorithms (Susskind et al., 2003) are not needed and retrievals can be performed on every pixel, or field of view (FOV), rather than on the nine pixel field of regard (FOR). This allows for retrievals from AIRS with a 15 km rather than 45 km minimum footprint, which was the resolution for the earlier NH_3 retrievals from AIRS obtained by Warner et al. (2016) using cloud cleared radiances.

MUSES uses the Optimal Spectral Sampling (OSS) model (Moncet et al., 2008) as its forward model; OSS is a fast and accurate radiative transfer method designed specifically for the modeling of radiances measured by sounding radiometers in the infrared, although it is applicable throughout the microwave, visible, and ultraviolet regions.

Since the retrieval is non-linear, an a priori constraint is used for estimating the true state (Bowman et al., 2006). If the estimated (retrieved) state is close to the actual state, then the estimated state can be expressed in terms of the actual state through the linear retrieval (Rodgers, 2000):

$$\hat{\boldsymbol{x}} = \boldsymbol{x}_a + \mathbf{A}(\boldsymbol{x} - \boldsymbol{x}_a) + \mathbf{G}\boldsymbol{n} + \mathbf{G}\mathbf{K}_b(\boldsymbol{b} - \boldsymbol{b}_a) \quad (1)$$

where $\hat{x}$, x_a, and x are the retrieved, a priori, and the "true" state vectors respectively, **G** is the gain matrix, $\boldsymbol{b}$ is the vector that contains parameters not retrieved in the current step and $\boldsymbol{b_a}$ the a priori values for these parameters if they are retrieved in another step.

The averaging kernel, **A**, describes the sensitivity of the retrieval to the true state:

$$\mathbf{A} = \frac{\partial \hat{x}}{\partial x} = (\mathbf{K}^T \mathbf{S}_n^{-1} \mathbf{K} + \mathbf{S}_a^{-1})^{-1} \mathbf{K}^T \mathbf{S}_n^{-1} \mathbf{K} = \mathbf{G}\mathbf{K} \quad (2)$$

where S_n is the instrument noise covariance matrix, and S_a is the a priori covariance matrix for the retrieval. The Jacobian, **K**, is the sensitivity of the forward model radiances to the true state vector, $\boldsymbol{K = \partial L / \partial x}$ .The rows of **A** are functions with a finite width corresponding to the vertical resolution of the retrieved parameter. The sum of each row of **A** provides a measure of retrieval information that comes from the measurement (Rodgers, 2000) at the corresponding altitude, provided that the retrieval is quasi-linear. The trace of the averaging kernel matrix gives the number of degrees of freedom for signal (DOFS) from the retrieval.

The total a posteriori error covariance matrix S_x for a given retrieved parameter $\hat{x}$ is given by:

$$\boldsymbol{S_x = (A - I) S_a (A - I)^T + G S_n G^T + G K_b S_b (G K_b)^T} \quad (3)$$

where $\mathbf{S_b}$ is the expected covariance of the non-retrieved parameters. The total error (or uncertainty) for a retrieved profile is expressed as the sum of: i) the smoothing errors (first term on the right-hand-side), i.e. the uncertainty due to unresolved fine vertical structure in the profile; ii) the measurement errors (second term) originating from random noise in the spectrum; and iii)

the systematic errors (last term) due to uncertainties in the forward model parameters not retrieved in the NH_3 step, some of which are constant and some of which change from retrieval-to-retrieval (Worden et al., 2006). The MUSES NH_3 retrieval step includes the estimated errors in water vapor and temperature in the systematic errors. For the retrieved profiles used in this study the measurement error ranged from 3% to 23%, the systematic errors mainly from 1% to 60%, and the smoothing errors from 24% to 130%. Example retrieved profiles and corresponding errors are shown in Figure S3. By providing the expected error covariance and the averaging kernels, this approach facilitates the use of the retrieved profiles in inverse modeling efforts, since both terms are used to weight the information coming from the retrieval. The error covariance gives users an uncertainty estimate for each retrieved profile, which can be utilized to screen the data or be included in a statistical analysis. Furthermore, the estimated uncertainty derived from the error covariance can be compared to measured uncertainties, obtained by calculating the spread of the differences between satellite and in situ data, as will be shown in sections 4.1 and 4.2; this analysis can indicate if there are error terms missing from the optimal estimation formulation. Note that the estimated error cannot account for sampling errors, i.e., differences between the air masses sampled by the satellite and by the in situ instruments, or sub-pixel variability

Rodgers and Connor (2003) presented a method for comparing satellite profiles of trace gases with limited vertical resolution with in situ profiles obtained on a much finer grid. This approach is often described as "applying the instrument operator" or "applying the averaging kernel". It attempts to estimate how the space based instrument would "see" an in situ profile by applying the equation below to the in situ data:

$$\mathbf{X} = \mathbf{X}_{apriori} + \mathbf{A} \left(\mathbf{X}_{aircraft} - \mathbf{X}_{apriori} \right) \quad (4)$$

The estimated profile **X** has been smoothed by the operator, simulating the smoothing due to the coarser resolution of the satellite observation. When X is compared to the satellite observations it is assumed that the smoothing error has been accounted for and can be ignored, which is not the case when satellite observations are compared directly to measured profiles; the remaining errors will be due to instrument noise and temporal and spatial sampling differences; the latter can be especially large for NH_3, due to its large variability, as was discussed above. We will follow the Rodgers and Connor approach as described above, as it is the optimal method for taking into account the sensitivity of the instruments; however, as a way introducing the data while also demonstrating the pitfalls of not considering the different vertical resolution of the satellite and aircraft data, we will also show simple differences between the aircraft and satellite data.

A note on applying the operator: AIRS and CrIS profiles extend to the top of the atmosphere, while the aircraft profiles used here rarely go above 700 hPa in California and 500 hPa in Colorado. We have extended the aircraft profiles by blending in the MUSES a priori profile above the top of the aircraft profile, then applied the instrument operator to these extended profiles.

2.2 MUSES data

2.2.1 AIRS single pixel NH_3 retrievals

AIRS is a nadir-viewing, scanning thermal infrared (TIR) spectrometer launched on board the Aqua satellite on May 4, 2002, into a sun synchronous polar orbit at an altitude of 705 km with a 1:30 am local solar time (LST) Equator in the ascending node and 1:30 pm (LST) in the descending node (Aumann et al., 2003). The daytime overpass is an ideal time for NH_3 retrievals, as thermal contrast is high and emissions are usually peaking, driven by higher temperatures. AIRS measures the thermal radiance between 3–12 microns with a spectral resolution of ~ 0.75 cm^{-1} and a noise

level of ~ 0.15K at 270 K (Zavyalov et al., 2013) in the 970 cm^{-1} NH_3 absorption window. A single AIRS FOV has a circular footprint with ~15 km diameter at nadir and the AIRS swath width is ~1650 km, which enables near global coverage twice daily.

2.2.2 CrIS single pixel NH_3 retrievals

CrIS is a Fourier Transform Infrared Radiometer (FTIR) launched on the Suomi National Polar Orbiter Preparatory (SNPP) platform in October 2011 into sun-synchronous orbits (824 km altitude) with the same LST crossing times as AIRS (1:30 pm and 1:30 am). CrIS was also deployed on the Joint Polar Satellite System (JPSS-1) in November 2017 and on JPSS-2 in November 2022, but in this paper only CrIS data from the SNPP platform have been used. CrIS is a cross track scanning instrument with a 2200 km swath width (+/- 50 degrees) with 14 km circular pixels (at nadir), a spectral resolution of 0.625 cm^{-1} and low spectral noise (~0.04 K at 270K) (Zavyalov et al., 2013) in the NH_3 spectral window. CrIS also provides twice daily global coverage. Note that in this paper there is a data gap in the SNPP-CrIS record between March and June 2019, corresponding to a malfunction in the electronics during that time.

While both AIRS and CrIS have the same equatorial crossing time, this does not imply that both instruments are observing the same location at the same time at the same angle. For example, on January 22, 2013, CrIS flew almost directly over the Central Valley around 2100 UTC, while AIRS had its closest observation 15 degrees to the west around 2200 UTC, near the edge of its swath. Therefore, the set of aircraft profiles co-located with each instrument is not identical.

3. Data

3.1 Aircraft Data

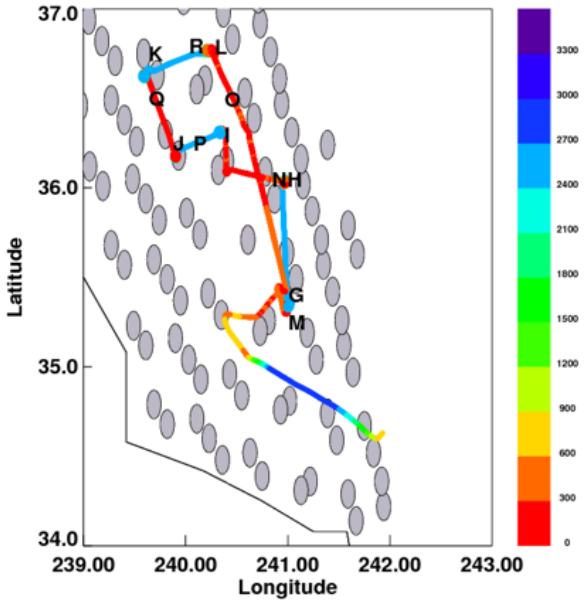

Figure 1: Sample aircraft track during DISCOVER-AQ in the Central Valley, CA; colors indicate altitude, letters locations of aircraft spirals; CrIS pixels are shown as grey ellipses

The NASA DISCOVER-AQ (Crawford and Pickering, 2014) campaigns were designed to validate collocated satellite observations of atmospheric pollutants over four regions in the United States: (Maryland/Washington D.C, California, Texas and Colorado), but NH_3 was only measured in California and Colorado. Vertical profiles of NH_3 were obtained by the PTR-MS instrument (Müller et al. 2014) deployed aboard the NASA P3B aircraft during the California campaign in January and February 2013 and in Colorado in July and August 2014 in Colorado in 2014. The P3B flight pattern was specifically designed for satellite validation: the aircraft flew repeated upward and downward spirals, typically 5 km wide connected by transects. An example trajectory, overlaid on the locations of CrIS NH_3 retrievals, is shown in Figure 1: the aircraft altitude is indicated by the colors, and the locations of the spirals are marked with letters. Note that the PTR-MS instrument samples the atmosphere at 1Hz but the data in Figure 1 were binned over 100 m to improve visibility. The estimated instrument uncertainty is 35% (Müller et al., 2014). However, the PTR-MS NH_3 data were a side product of the PTR-MS measurements during DISCOVER-AQ, which were designed to obtain data on volatile organic compounds (VOCs). NH_3 is sticky and accumulates in the instrument inlet, slowing the instrument response This effect leads to biases if the NH_3 amounts are changing rapidly (Sun et al., 2015);when the aircraft is leaving the boundary layer on upward spirals the instrument does not respond quickly enough to the sharp

365 decrease in NH_3 and overestimates the NH_3 concentration; similarly, when entering the boundary layer on downward spirals, the response to the increase in NH_3 is slow, and NH_3 is underestimated (see Figure 9 in Guo2021). Furthermore, the detection limits for NH_3 were much higher than for the VOCs that were the primary target of the PTR-MS measurements: 7.0 ppbv in California and 3.0 ppbv in Colorado (Armin Wisthaler, personal communication). These limits
370 imply that any aircraft observations below these values are effectively noise.

3.2 Ground Data

The USDA-ARS Northwest Irrigation and Soils Research Laboratory established a regional NH_3
375 monitoring network in the Magic Valley region of south-central Idaho, USA utilizing the NADP AMoN (Puchalski et al., 2015) network technology and protocols, but with much greater spatial density. The network measured ambient NH_3 concentrations along two transects of the Magic Valley (North-South) and West-East) utilizing passive diffusive NH_3 samplers collected on a bi-weekly basis from February of 2018 through December of 2020. The objective of the project was
380 to determine the spatial variability of ambient NH_3 concentrations across the region, which is dominated by agricultural production and high-density dairy operations, to better understand the potential for NH_3 transport within and downwind of the region.

4.0 DISCOVER-AQ Analysis

The DISCOVER-AQ campaigns in California and Colorado provide the most comprehensive set
385 of in situ NH_3 profile data available (as opposed to retrievals from FTIR instruments). Both locations have many strong sources and each campaign carried out multiple flight days over a two month period. These datasets demonstrate the strengths and limitations of satellite data in areas of great interest to the air quality community; additionally, they allow for the evaluation of the accuracy of the retrieval estimated error, as calculated from Equation 3. During each flight

390 the aircraft flew multiple up and down spirals. The satellite profiles were co-located with aircraft profiles taken within one hour of the satellite overpass time and 15 km of the pixel center, the same criteria used by Guo 2021.This co-location criterion is much stricter than is usual for satellite validation (see Hegarty et al., 2022 for an example with CO retrievals from AIRS, which used nine hours and 50 km) but is necessary given the short lifetime of NH_3 (on the order of
395 hours to days) due its high reactivity and fast deposition. In fact Tournadre et al. (2020) used an even stricter time requirement of 30 minutes for comparing FTIR and IASI NH3 retrievals over Paris, but we found that such a limited time window drastically reduced the available data. Given the chosen criteria, each CrIS or AIRS profile was compared with data from at most two spirals. Retrievals were checked for quality by ensuring that for all retrievals the root mean square error
400 (RMSE) of the residuals was less than 5.0. The MUSES cloud optical depth (COD) values were also evaluated but since the maximum COD for the retrieved profiles was 0.25 no retrievals were rejected due to large COD. Four CrIS profiles over Colorado were rejected due to very high estimated uncertainties. The DOFs ranged were between 0.8 and 1.1, except for two CrIS profiles over California, four AIRS profiles in California and six AIRS profiles in Colorado, for
405 which the DOFS were smaller (0.2 to 0.7). Given the small number of profiles in each dataset, we did not exclude any profiles based on the DOFs.

Comparing the aircraft and satellite profiles requires regridding the aircraft data to the satellite vertical grid. This was accomplished by defining layers centered around each AIRS/CrIS level, then finding the median value of the aircraft profile in each layer. The lowest layer extended
410 from the surface to the mid-point between the surface and the first AIRS/CrIS level above the surface. The CrIS retrieval layers are fairly coarse and therefore the median value of the PTR-MS is derived from a set of hundreds of measurements spanning the layer, and from both up and

down flight paths, thus possibly reducing to some degree the biases from entering and leaving the boundary layer discussed above. In the California campaign the average height of the mixed layer was around 500m and never exceeded 1km (~ 900 hPa), so these biases were only present in the layer centered around this level, where levels of NH_3 (5-40 ppbv) are still high. On the other hand, in Colorado the average height of the boundary layer was around 3km (~700 hPa), and therefore the biases were present in a layer with lower levels of NH_3 (0-5 ppbv). Example plots of the distribution of the aircraft data in each layer (Figure S4) demonstrate the variability in these data, and that the median and mean do not always coincide, indicating a non-Gaussian distribution of the measurements in these cases and therefore suggesting the use of the median as as the most appropriate metric.

4.1 California

DISCOVER-AQ in California took place during January and February of 2013. The Central Valley is one of the strongest NH_3 source regions in North America (e.g., Clarisse et al., 2009, Shephard et al., 2020), and this was reflected in the aircraft data, which registered near surface amounts as high as 100 ppbv (Figure 2, upper left panel). There were thermal inversions over the entire period (Figure 2, upper right), which lead to increased uncertainties in the retrieval, as they effectively created an emission layer above the surface, i.e., a layer that is warmer than the surface and therefore emits more than it absorbs. Inversions also limit the vertical extent of the boundary layer, with consequently lower NH_3 concentrations at altitudes where the retrieval has greater sensitivity. Nevertheless, evaluating the AIRS and CrIS NH_3 profiles against the aircraft data is a useful exercise, as the combination of inversions and strong sources is not a rare occurrence, and this analysis demonstrates both the capabilities and limitations of retrievals under these conditions.

43 AIRS and 58 CrIS profiles met the co-location criteria described above. Before applying the instrument operator as described in section 2.1, we directly compare the satellite data against the aircraft profiles (Figure 3a and Figure 3b). This is done to introduce the satellite data, and to demonstrate to users unfamiliar with the instrument operator the importance of accounting for the different vertical resolution of the remote and in situ instruments through the use of the operator. Both instruments showed large negative biases near the surface, as low as -80 ppbv for AIRS and -100 ppbv for CrIS, while the average bias at this level was ~-38 ppbv for AIRS and ~44 ppbv for CrIS, with a spread of ~ 24 ppbv and 38 ppbv, respectively (see Table I). This large negative bias is likely due to a combination of sub-pixel heterogeneity (Sun et al., 2015; Kille et al., 2019), the inherent difficulties of carrying out retrievals over thermal inversions, and systematic and smoothing errors (due to the different vertical resolution). Note that the mean CrIS value at the surface (~16 ppbv) is 60% greater than the AIRS value (~10 ppbv), while the reverse is true at 908 hPa (9.7 vs 7.6 ppbv). This difference can be attributed to the greater number (24 out of 43) of moderate (green curves) or background (blue curves) a priori profiles selected by the MUSES algorithm for the AIRS retrievals, when compared to CrIS (4 out of 48). The moderate and background a priori profiles and constraints drive the retrieval to distribute NH_3 more uniformly over the vertical range, rather than concentrating it near the surface. For either instrument the surface mean value is much lower than the PTR-MS mean (~37 ppbv), consistent with the large biases noted above, though the CrIS mean value (~16 ppbv) is just within the standard deviation of the PTR-MS data. Clouds are accounted for in the MUSES retrieval (Kulawik et al., 2006) and thus cloudy conditions should not significantly impact the NH_3 retrievals. Both the bias and the spread drop significantly with increasing altitude, as do the measured concentrations; while the biases decrease, they become positive and are not

insignificant at 825 hPa (~30% at 825 hPa), and the spread is quite large (~100%). However, at this level, which is above the MLH for all flight days, many of the aircraft observations are below the detection limit of the PTR-MS (see Figure S5) and are thus highly uncertain.

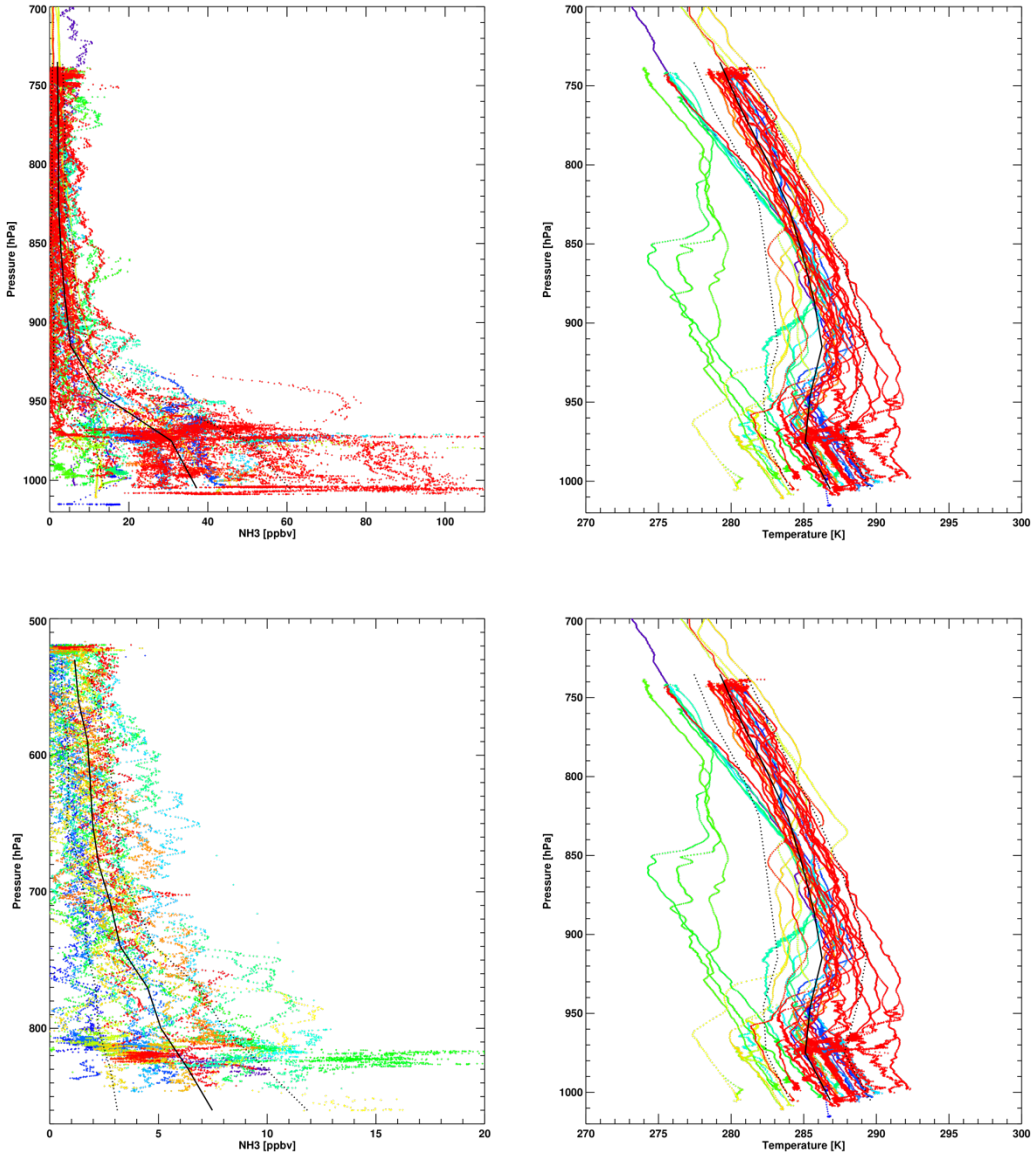

Figure 2: NH_3 profiles (left) obtained from aircraft during DISCOVER-AQ in California (top) and Colorado (bottom); only profiles co-located with CrIS data are shown; corresponding temperature profiles (right). Black solid line indicates the mean, black dashed lines the standard deviation.

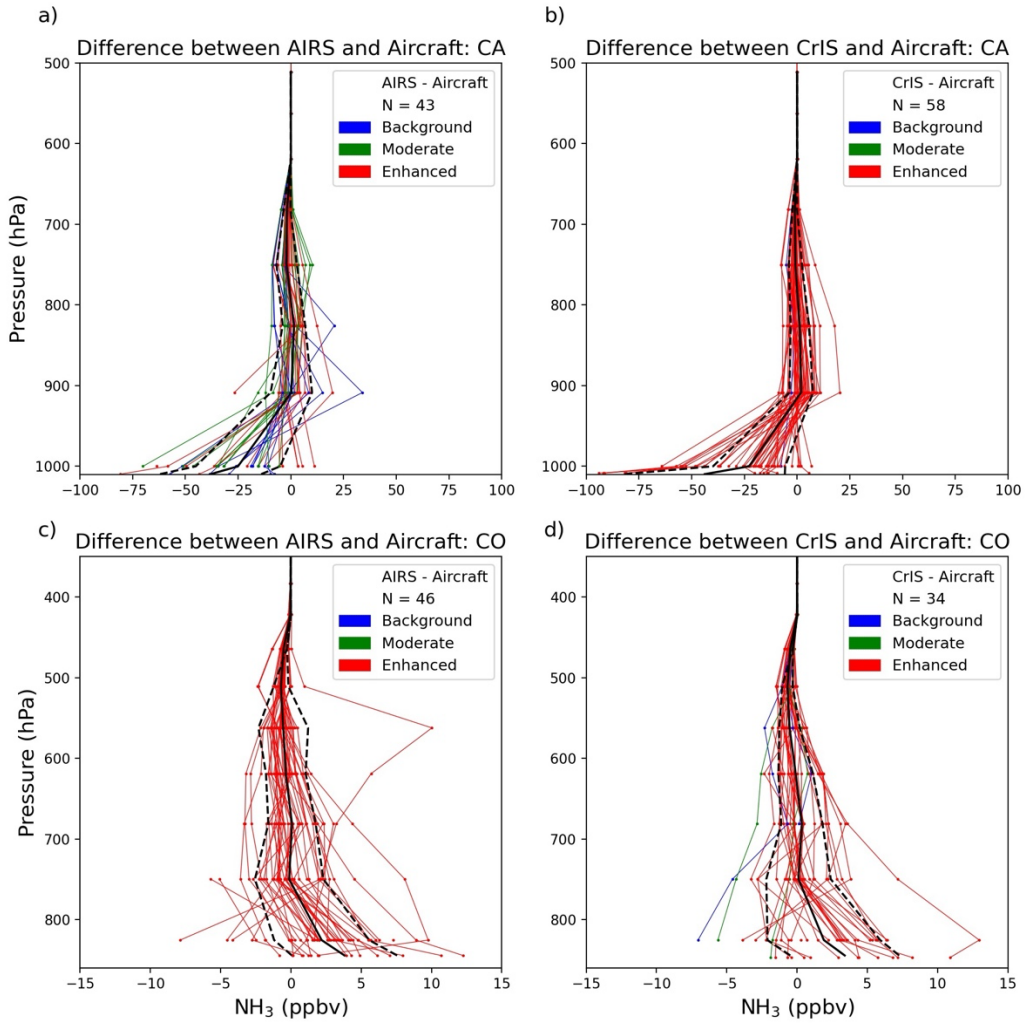

Figure 3: Difference between AIRS and aircraft NH_3 profiles (left) and CrIS and aircraft (right) during DISCOVER-AQ in California (top) and Colorado (bottom); solid line indicates mean bias and dashed lines standard deviations. Colors indicate choice of a priori profile.

Therefore it become impossible to make any quantitative statements about the differences between the satellite and aircraft data at these higher altitudes.

The sum of the rows of the averaging kernels (SRAK) (Figure 4,), which provides an estimate of the retrieved information at each level originating from the measurement rather than from the a priori, shows for both AIRS and CrIS that while the information from the radiance data peaks just below 700 hPa, it also significantly contributes to the retrieved surface values. This is driven

by the structure of the covariance matrix (S_a). As noted in the introduction of the DISCOVER-AQ section, the DOFS for AIRS and CRIS NH3 ranged mostly between 0.8 and 1.0, signifying the retrieval provides only one piece of information, basically a column amount. By building off-diagonal correlations in a priori covariance matrix between the surface level and a few levels above, this information is vertically distributed in such a way that it restricts unphysical oscillations in the retrieved profile and deviations a priori profile shape. Each of the three a priori profiles is associated with a different covariance matrix. The enhanced a priori retrieval tends to load the profiles at the surface, while the moderate and background profiles push NH3 to the free troposphere. The maximum SRAK (~1.2-1.3) is similar for both sensors, as is the SRAK at the surface (~0.6). However, there is much greater variability in the AIRS SRAK, possibly due to higher instrument noise.

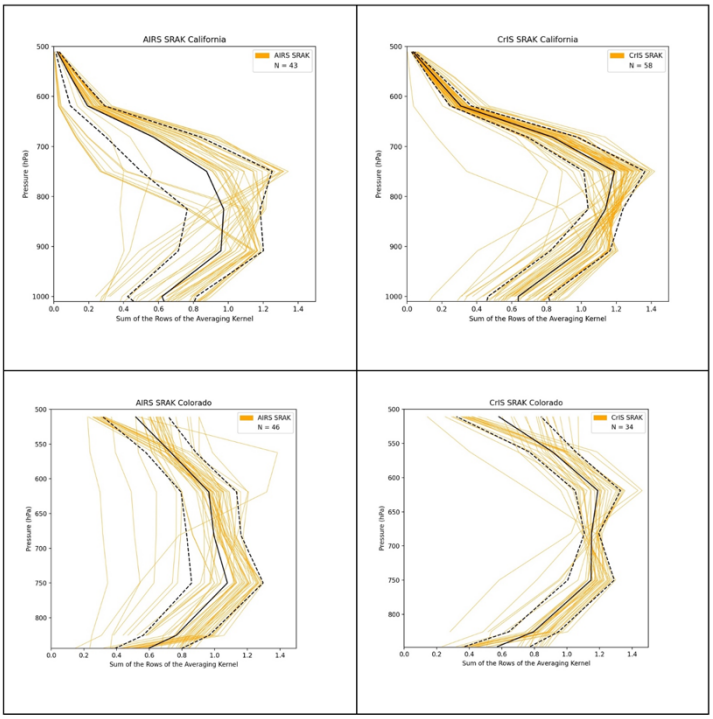

Figure 4: Sum of the row of the averaging kernels (SRAK) for AIRS (left panels) and CrIS (ritght panesls);California (upper panels) and Colorado (lower panels)

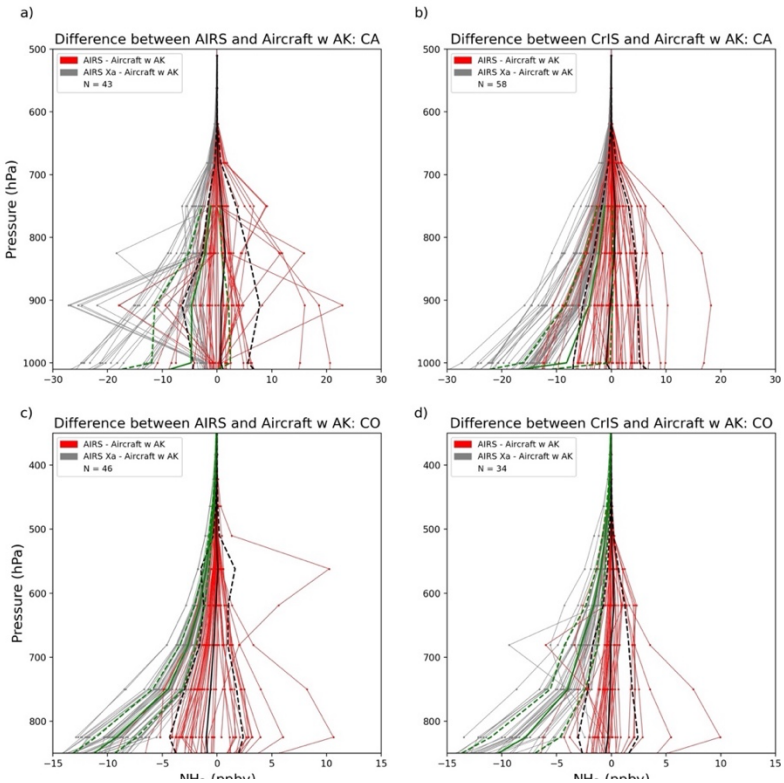

Figure 5: Difference between AIRS and aircraft NH3 profiles (left) and CrIS and aircraft (right) during DISCOVER-AQ in California (top) and Colorado (bottom); the averaging kernel has been applied to the aircraft data; red lines show differences between the retrieved profiles and the aircraft data, black solid lines indicate mean bias and black dashed lines standard deviations; grey lines show differences between the a priori profiles and the aircraft, green solid lines indicate mean bias and green dashed lines standard deviations.

Applying the instrument operators following equation 4 (Figure 5a and Figure5b), red and black curves) eliminates the smoothing error, which reduces the bias at all levels to close to or less than 1.0 ppbv (Table 1, top section), roughly 7% to 10 % of the surface value, increasing to 20% at 825 hPa, indicating that the large differences seen in the direct comparison are due mainly to the inability of the satellite instruments to resolve the fine vertical structure of the profile; the standard deviation is also reduced, especially at the lower levels, but is not eliminated, which suggests that other error sources are present. If instead the a priori profiles are compared with the aircraft data, we see a large negative bias near the surface (~-9 ppbv for AIRS and ~-18 ppbv for CrIS). This result demonstrates that the retrieval process does add significant information and reduces the a priori error.

A great benefit of the optimal estimation approach is that is provides both retrieved profiles and estimated errors. If these errors are lower than the error relative to the in situ or model data, they indicate that some error sources have not been accounted for in the retrieval. Here we compare the sum of the measurement and systematic errors from Equation 3 (Figure 6a and 6b, red and blue curves) against the measured uncertainties (the fractional standard deviation derived from the standard deviations of the differences in the "Satellite-Aircraft with AK" column in Table 1) (Figure 6a and 6b, black curve), which have the smoothing error removed by the application of the averaging kernel, A. Since the measurement error is usually quite low (see Figure S3 for examples) the estimated uncertainties are nearly equivalent to the systematic errors, and thus represent the estimate of the error in NH_3 due to errors in temperature and water vapor. The average estimated uncertainties are below the measured uncertainties for both AIRS and CrIS, confirming that some error sources are not accounted for in the optimal estimation process.

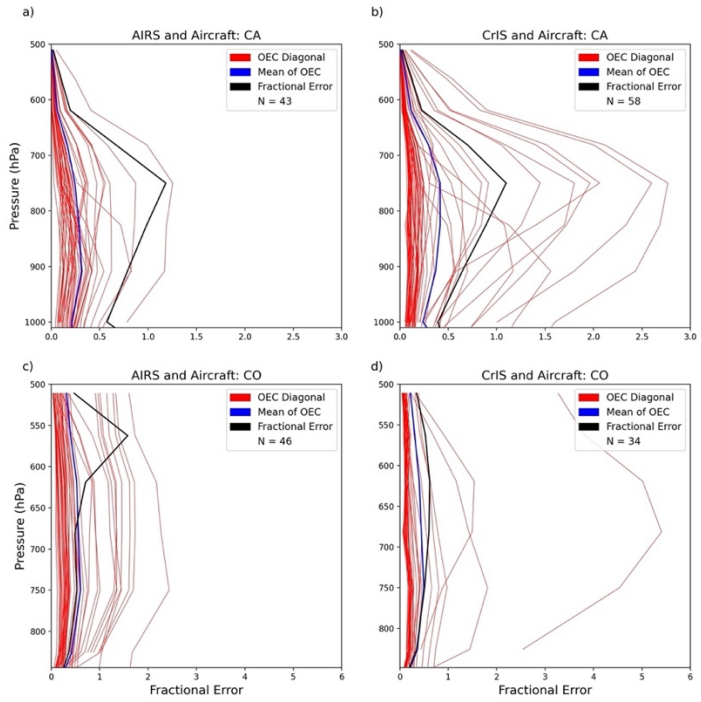

Figure 6: Fractional standard deviation between AIRS (left) and CrIS (right) and aircraft profiles with the averaging kernel applied (black) during DISCOVER-AQ in California (top panels) and Colorado (bottom panels); estimated uncertainty (red) and mean of estimated uncertainty (blue).

A possible candidate is the sampling difference: AIRS and CrIS sampled three dimensional columns, 15 to 50 km wide, while

aircraft instruments sampled in two dimensions, vertically and along a spiral line with a 5 km width. Sub-pixel variability likely also contributes to these errors. The estimated uncertainties range in general from 5 to 50% at the surface, though five cases had significantly larger errors. At 850 hPa the variability in the uncertainties is much larger, ranging from 10% to 250%, strengthening the argument that it is not possible to carry out a meaningful comparison at this altitude or higher with this dataset.

Table 1: Statistical analysis of the DISCOVER-AQ data from AIRS, CrIS and the aircraft over California in 2013 and Colorado in 2014.

California												
	Profile				Satellite-Aircraft: no AK				Satellite-Aircraft: with AK			
	Mean		Std Dev		Bias		Std Dev		Bias		Std Dev	
Pressure	AIRS	CrIS	AIRS	CrIS	AIRS	CrIS	AIRS	CrIS	AIRS	CrIS	AIRS	CrIS
hPa	ppbv	ppbv	ppbv	ppbv	ppbv	ppbv	ppbv	ppbv	ppbv	ppbv	ppbv	ppbv
1008.486	9.69	16.211	10.785	6.027	-38.03	-43.799	23.972	37.988	1.124	-0.279	5.6	6.723
1000	9.342	14.443	9.875	5.44	-25.049	-22.746	19.995	17.106	0.664	-0.89	5	6.046
908.514	9.693	7.63	8.634	4.101	0.238	1.956	9.81	5.582	0.691	-0.159	7.08	5.015
825.402	5.742	4.883	5.401	3.372	1.471	1.266	5.327	4.345	1.511	0.593	4.169	3.815
749.893	3.083	2.958	3.47	2.311	-1.96	-0.801	4.815	3.101	0.883	0.729	2.605	2.446
681	0.979	1.195	0.814	0.664	-1.78	-1.083	1.597	1.111	0.156	0.21	0.551	0.689
618.966	0.244	0.357	0.149	0.083	0.046	0.038	0.057	0.076	0.008	0.014	0.046	0.078
Colorado												
	Profile				Satellite-Aircraft: no AK				Satellite-Aircraft: with AK			
	Mean		Std Dev		Bias		Std Dev		Bias		Std Dev	
Pressure	AIRS	CrIS	AIRS	CrIS	AIRS	CrIS	AIRS	CrIS	AIRS	CrIS	AIRS	CrIS
hPa	ppbv	ppbv	ppbv	ppbv	ppbv	ppbv	ppbv	ppbv	ppbv	ppbv	ppbv	ppbv
844.469	10.341	9.805	3.415	3.801	3.817	3.387	3.741	3.871	-0.89	-0.5026	2.884	2.133
825.402	8.214	7.529	3.064	3.595	2.19	1.902	3.377	4.006	-0.978	-0.292	3.355	2.723
749.893	3.889	3.852	2.173	2.101	-0.12	0.102	2.431	2.292	-0.592	-0.108	2.375	2.021
681.291	2.324	2.703	1.143	1.207	0.084	0.338	1.684	1.465	-0.315	-0.046	1.29	1.652
618.966	1.474	1.858	0.943	0.974	-0.356	-0.102	1.41	1.228	-0.099	0.262	1.115	0.983
562.342	1.07	1.104	1.444	0.548	-0.538	-0.535	1.764	0.724	0.084	0.159	1.557	0.498
510.898	0.521	0.552	0.231	0.212	-0.695	-0.687	0.523	0.374	-0.068	0.008	0.278	0.189

Much of the work on validating NH_3 from space-based infrared sensors has been done using IASI data, which provide total columns rather than profiles (e.g., van Damme et al., 2015a; Dammers et al., 2017; Guo2021), though Dammers et al., (2017) estimated IASI profiles by using two fixed vertical profiles to convert column amounts to profiles and thus to also obtain surface values. Guo2021 explored four approaches (see Guo2021 Figure5) for accounting for the NH_3 amount above the mixed layer height (MLH) and obtained the best agreement with IASI data by assuming zero NH_3 above the MLH (R=0.57 and slope=1.0). This is a fairly reasonable

assumption, since NH_3 has a short lifetime (on the order of hours or days), and is rarely transported to the middle or upper troposphere, except during strong fires; it has been measured above the mixed layer, but at low levels (less than 1 ppbv; e.g., Höpfner et al., 2019; Nowak et al., 2010). Here we compare AIRS and CrIS total columns with aircraft total columns calculated following two approaches. First we used the zero NH3 above the MLH approach adopted by Guo2021. In this procedure the in situ NH_3 total column is estimated by integrating the aircraft NH_3 profile to the top of the mixed layer; above this level, NH_3 amounts are assumed to be zero.

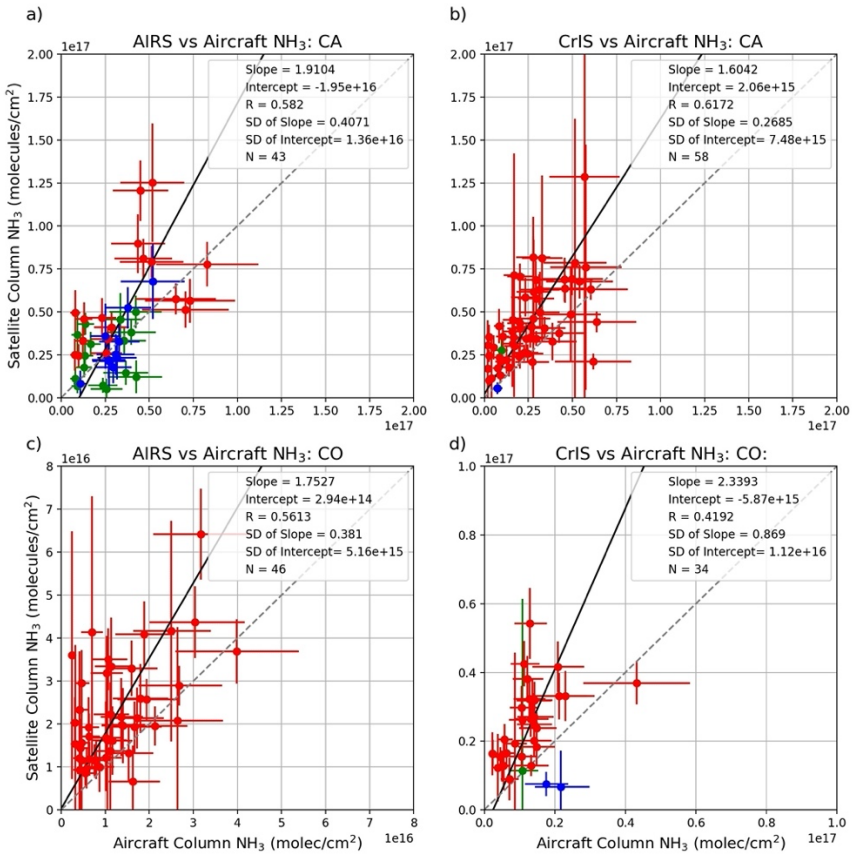

Figure 7: total NH3 columns from AIRS (left) and CrIS (right) versus aircraft columns during DISCOVER-AQ in California (top panels) and Colorado (bottom panels); dashedline shows the 1:1 lin, black line the linear fit; vertical and horizontal lines indicate the uncertainties in the aircraft and satellite data, respectively. Aircraft columns assume NH3 above top of MLH is zero. Colors indicate choice of a priori profile, as in Figure 3.

The MUSES total columns are compared against the integrated aircraft columns, using orthogonal linear regression (Figure 7a and 7b), again colored by the choice of the a priori profile; the intercept has been allowed to vary, as both AIRS and CrIS have detection limits, (~1.0 ppbv, for thermal contrast above 5K), as does IASI (3.0e15 molecules/cm2, for thermal contrast above 5K). Note that in this approach the instrument operators have not been applied to the aircraft column data. The correlation coefficients are 0.58 for AIRS and 0.62 for CrIS, within the range of results from previous studies (e.g., Dammers et al., 2016, found correlations ranging from 0.28 to 0.81 when comparing surface FTIR and CrIS columns). However, the slopes are very much greater than one (1.9 for AIRS and 1.6 for CrIS), which was not the case in the IASI evaluation of Guo2021. If this assumption of zero amounts NH_3 above the mixed layer is no longer valid at the later (13:30 LST) CrIS and AIRS overpass times, the aircraft columns would be biased low with respect to CrIS and AIRS; the profile differences shown in Table 1 also suggest that AIRS and CrIS are measuring more NH_3 above 910 hPa. Given the uncertainty in the aircraft measurements at these higher altitudes it is not possible to currently to determine the true NH_3 amounts above the mixed layer.

In the second approach (Figure 8) we calculate partial AIRS/CrIS columns by integrating the profiles to the MLH only. The results are interesting: the AIRS correlation (Figure 8a) decreases (from 0.58 to 0.46), and the slope drops from 1.9 to 1.4. These changes occur because many of the columns decrease substantially (note large group of values below 1.0e16 molecules/cm2). We found that these observations derive from profiles for which the retrieval selected a background or moderate prior. When a background or moderate prior is chosen, the retrieval distributes the NH_3 differently than if the enhanced prior is used (see Figure S3, two rightmost panels): in the moderate case the retrieval creates a profile that peaks around 900 hPa, while in

the polluted case the peak is at the surface. By limiting the integration to the top of the MLH a substantial fraction of the retrieved column from the AIRS observations is excluded for the profiles derived from the moderate prior. The slope of the CrIS comparison drops dramatically from 1.6 to 0.6, but the correlation actually increases slightly from 0.61 to 0.64. Visual inspection suggests that truncating the CrIS integration had a large impact on a few outliers but overall reduced most columns only slightly, since the bulk of the bulk of the NH_3 is below the MLH, and thus did not substantially affect the correlation. Both the AIRS and CrIS results demonstrate that the retrievals are showing a non-neglible amount of NH_3 above the mixed layer, more so for AIRS than for CrIS, but at present it is not possible to determine if these values are real, given the uncertainties in the aircraft data at these altitudes, or if they are the result of redistribution of NH_3 to higher altitudes driven by the a priori profile shape and error covariance.

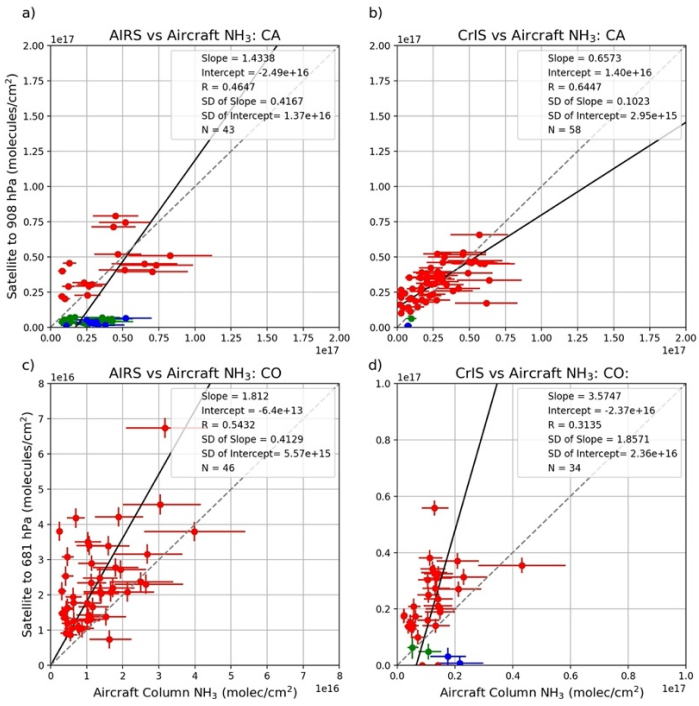

Figure 8: same as Figure 7, but AIRS/CrIS columns are partial columns, extending only to the top of the MLH.

4.2 Colorado

DISCOVER-AQ Colorado took place during July and August of 2014, in the Colorado Front Range; while this is also a region with strong NH_3 sources, the aircraft data showed lower values than in the California Central Valley (Figure 2, lower left panel); maximum values are on the order of 20 ppbv, with most near surface values ranging from 5 to 10 ppbv, above the uncertainty in the aircraft data, which was ~3ppbv in the Colorado campaign. In contrast to the Central Valley there were no thermal inversions during this period (Figure 2, lower right panel) and the MLH was much higher, about 3 km (~700 hPa) on average. Applying the co-location criteria yielded 46 AIRS profiles but only 34 CrIS profiles, in part due to some poor quality CrIS retrievals. Direct comparisons of the AIRS and CrIS profiles with aircraft data (Figure 3, lower panels) show both AIRS and CrIS biased high by 3.8 ppbv (AIRS) and 3.4 ppbv (CrIS) near the surface (~844 hPa) and by 2.2 ppbv (AIRS) and 1.9 ppbv (CrIS) at 825 hPa, but the bias is close to zero at 750 hPa. Note that this is in direct contrast to the California results, which showed both AIRS and CrIS NH_3 biased very low at and near the surface and biased slightly high at greater altitudes. However, here too the mean AIRS (10.3 ppbv) and CrIS (9.8) surface values are within the standard deviation of the aircraft data.

The sum of the rows of the averaging kernel plots (Figure 4, lower panels) present similar maximum and surface values as in California, and again applying the instrument operator reduced the bias to below 1.0 ppbv (~10%) , but did not reduce the spread in the satellite-aircraft differences dramatically (Figure 5a and Figure 5b), while the large bias seen against the a priori profiles (~-12 ppbv for AIRS and ~-10 ppbv for CrIS) is removed by the retrieval, confirming again that the retrieval process provides information content beyond the a priori.

The uncertainty analysis (Figure 6a and Figure 6b) shows that in the region where both the satellite and aircraft observations are reasonably robust, the estimated uncertainty is quite close to the measured uncertainty below 700 hPa. Finally, the total column comparisons also indicate that the AIRS and CrIS NH_3 (Figures 7c and 7d) columns are correlated with the aircraft values (with correlation coefficients of 0.56 for AIRS and 0.42 for CrIS), but are biased high, most notably for CrIS, for which the regression presents a slope of 2.3. The AIRS total columns (Figure 7c) and partial columns (Figure 8c) are very similar, indicating the most of the retrieved NH_3 is below the MLH; since all AIRS retrievals used the enhanced prior, which concentrates NH_3 in the surface layer, this is to be expected. The CrIS partial columns (Figure 8d) show marked reductions in the smaller column values, which increase the slope from 2.4 to 3.5, and reduce the correlation to 0.31. These smaller columns correspond to retrievals that used background or moderate a priori profiles, and, as was described in the California section, push NH_3 higher up in the column, and are thus more sensitive to truncation. The fact the columns from the satellite instruments are much higher than the aircraft columns is possibly due to NH_3 produced by fires and lofted above the MLH, which were not measured by the PTR-MS but would be detected by AIRS/CrIS and redistributed downwards by the retrieval, leading to the high biases seen in the surface values before applying the instrument operator.

5.0 Magic Valley Analysis

5.1 USDA network

The USDA-ARS established and maintained an NH_3 monitoring network along two transects (North-South and West-East) across the Magic Valley region of south-central Idaho during the February 2018-December 2020 period (Figure 9). The Magic Valley region is heavily dominated

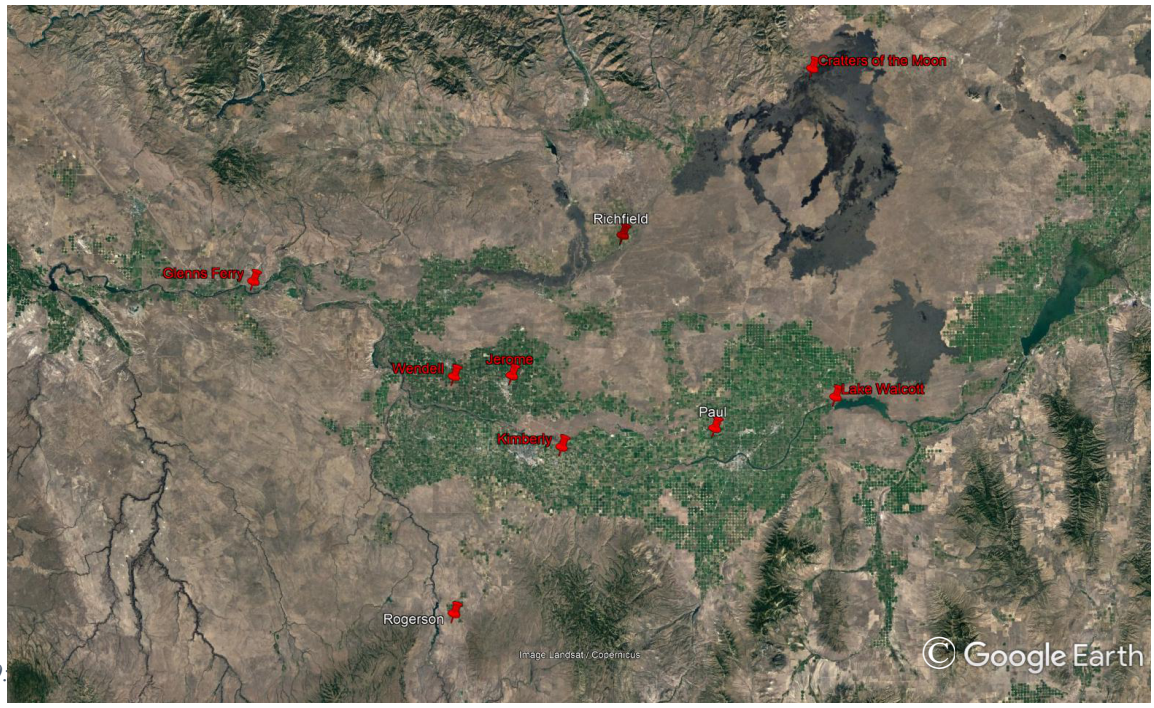

Figure 9.

by irrigated agriculture and is one of the most concentrated dairy production regions in the US. Research in this region has reported that NH_3 emissions from agricultural and dairy production contribute approximately 44,000 MT N yr^{-1} to the atmosphere (Leytem et al., 2021) and that NH_3 emissions fluctuate by season following trends in temperature (Leytem et al., 2011, 2013). The network was established to gain a better understanding of the spatial variablity of ambient NH_3 concentrations and transport within the region. The network consisted of 8 sampling locations (7 until 2020, when an additional site was added), and also utilized data from the NADP AMoN site located to the north of the region at Craters of the Moon National Monument. Ammonia concentrations were measured with passive diffusive NH_3 samplers (Radiello), which were deployed bi-weekly, and generated two week mean surface NH_3 concentrations. Radiello samplers have been shown to be approximmately 9% biased low (Puchalski et al., 2015). These data provided a unique opportunity to evaluate the seasonal signals measured by CrIS NH_3, as well as its capability to capture small scale (on the order of a few kilometers) spatial variability.

5.2 Evaluating CrIS NH_3 against the surface data

CrIS SNPP NH_3 data are available for most of the 2018-2020 period, with a gap in the spring of 2019 due to an instrument malfunction. Surface CrIS data within 15 km of each site were compared with the ground data at that site. Profiles with RMSE greater than 5.0 were excluded from the time series, as were clouds with COD greater than 1.0. Only the CrIS observations at CrIS ~13:30 LST were analyzed. The NH_3 retrievals at 1:30 LST have weaker signals (due to lower thermal contrast), and would add uncertainty to the results. While there are strong diurnal cycles in the NH_3 emitted from the dairy facilities (Leytem et al., 2011, 2013) the average daily emissions and temperatures, which strongly control the emissions, are close to the early afternoon values. Ideally one would use measurements of the daily cycle in NH_3 concentrations, to estimate the ratio between the 13:30 and 24 hour mean concentrations, as was done by Pinder et al. (2011), but such data are not available for the Magic Valley site. Figure 10 shows the individual CrIS observations (small red triangles), the two-week averages of the CrIS data (large red triangles connected with a red line) and the ground data (blue triangles) at each site.

The time series in Figure 10 are sorted by the peak values of the ground data. At every site, CrIS clearly captures the seasonal cycle, though winter values are usually underestimated: this can be attributed to weak radiative signals due to low temperatures and low thermal contrast. The CrIS level of detectability is normally cited as ~1.0 ppbv (Shephard and Cady-Pereira, 2015), but at low thermal contrast this level increases significantly. A few strong warm season peaks in the ground data are also not captured. At Craters of the Moon, a National Monument, and at Rogerson, in land administered by the Bureau of Land Management, CrIS returns consistently higher values than the ground site during the warmer months (May to October). At present we have no definitive explanation for this high bias. At the next four site (Glenns Ferry, Richfield,

Lake Wolcott and Kimberley), which are in areas of mixed agricultural activity, CrIS and the ground data are in good agreement during the warmer months, though CrIS underestimates the June 2018 maximum at the Richfield site. At all four sites there is a peak in the ground data in November 2019 that is either matched in the CrIS data (Glenns Ferry) or at least visible (Richfield, Kimberley, Lake Wolcott). This peak is also evident in the data from Paul and possibly Wendell, though the variability at this latter site makes it difficult to confirm. This suggests an area wide change in meteorological conditions, such as an inversion, that led to increased NH_3 near the surface: however, there is no evidence in the meteorological data for such an inversion. The last three sites (Paul, Jerome and Wendell) are close to and/or downwind of multiple dairies, which likely leads to greater sub-pixel inhomogeneity. CrIS underestimates the warm season maximum, and does not capture many of the peaks in the ground data, most notably at the Wendell site, where CrIS did not observe the over 80 ppbv peaks in 2018 and 2019.

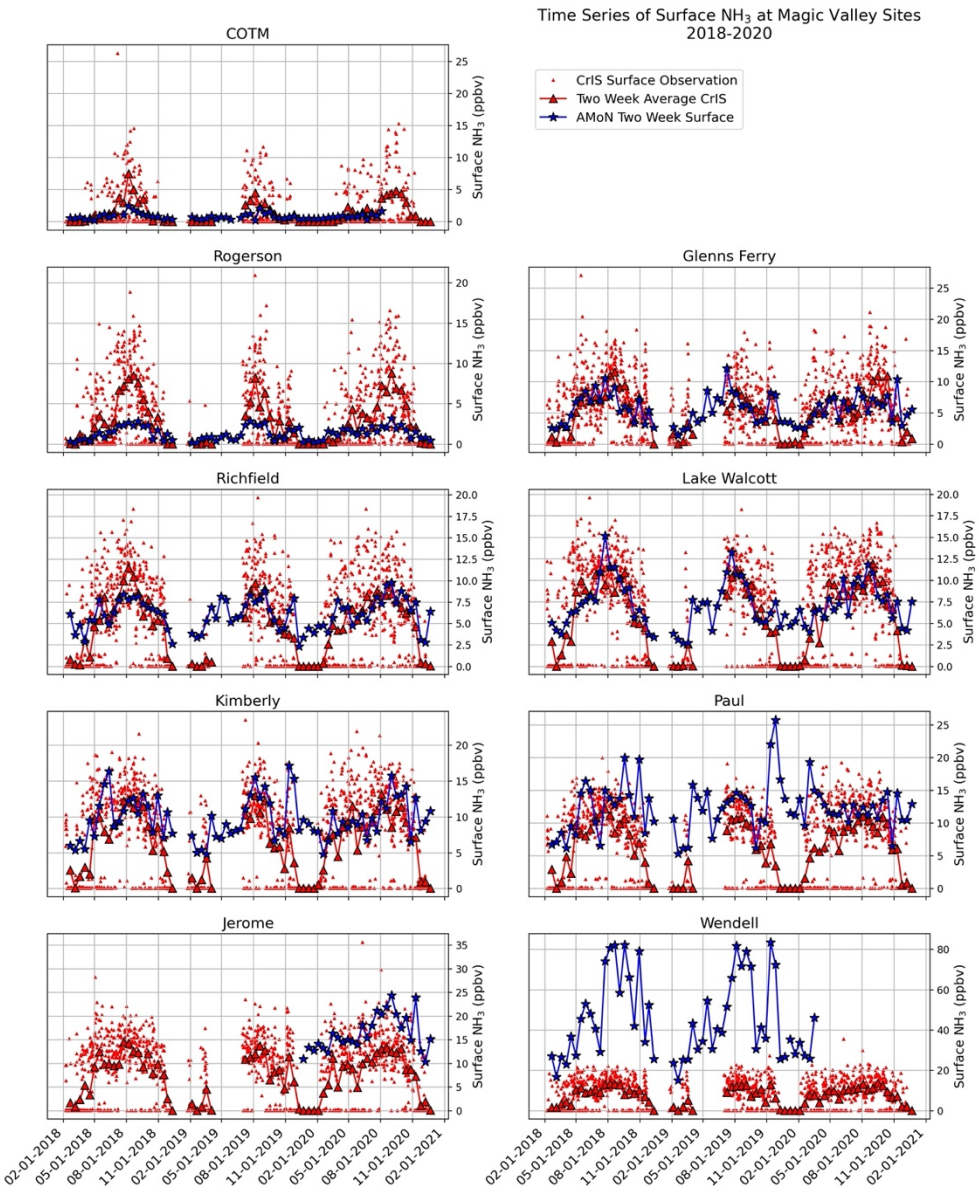

715 *Figure 10: Time series of the in situ data (blue triangles, and the collocated CrIS surface values; red dots indicate daily values, red triangles two week means.*

Analyzing these data in aggregate, first spatially then temporally, provides some useful insights.

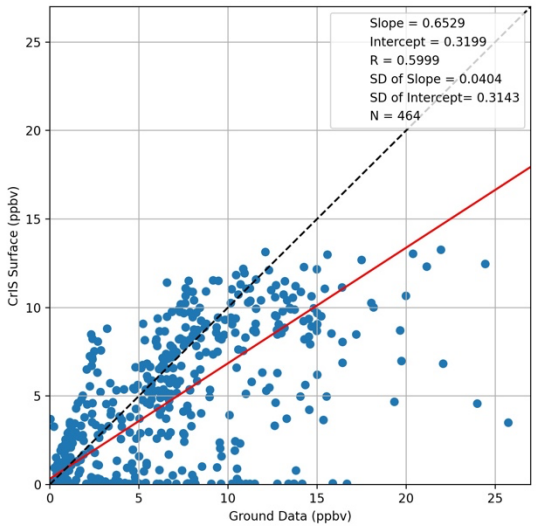

Figure 11: two week means of surface NH3 from CrIS and the in situ instruments; dashed line shows the 1:1 line, red line the linear fit.

Plotting the CrIS two week averages against all the ground data values (Figure 11), and excluding CrIS data with cloud OD greater than 2.0, along with the data from the Wendell site, which are extreme outliers, shows a correlation of 0.6, at the high end of the values reported in the literature (e.g., see van Damme et al., 2015b, as noted in introduction) and slope of 0.65, indicating that CrIS NH_3 is biased low overall. This result is in line with the low biases found in the surface values of the AIRS and CrIS California data, though here not necessarily caused by thermal inversions, and with the low biases in the CFPR results at high NH_3 FTIR values seen by Dammers et al. (2017). It provides a quantitative measure of the agreement seen in the seasonal cycles shown in Figure 10.

Three years of fairly dense data over a region with many sources with fixed locations are an excellent candidate for spatial oversampling algorithms, which trade temporal resolution for greater information on spatial variability. Here we applied the physics based oversampling algorithm developed by Sun et al. (2018), which uses the instrument spatial response function to weight the contributions of each satellite observation to a fine grid (here 0.002 deg), to each of the three years of CrIS data taken over the Magic Valley region (Figure 12). The in-situ data are overlaid on the CrIS maps; note that the Wendell values are shown in the upper right corner of

the maps, as otherwise they would distort the color scale; note also that the Jerome data are blank in 2018 and 2019, when this site was not operational.

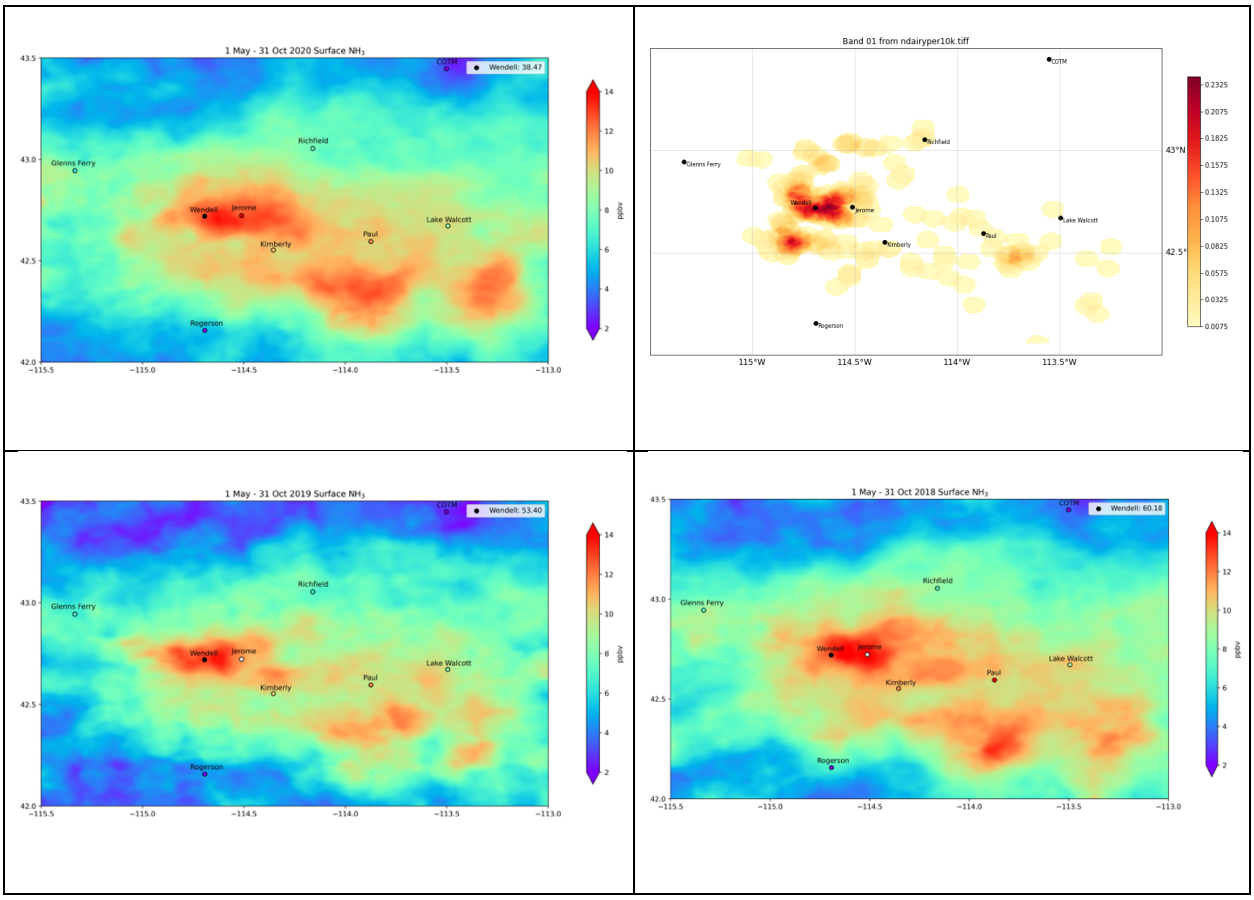

Figure 12: CrIS surface NH3 data from the May to October period oversampled onto a 0.002 deg grid for each of three years: 2020 (upper left), 2019 (lower left), 2018 (lower right); number of dairies per square kilometer (upper right)

The location of the CrIS NH_3 "hotspots" and the gradients in NH_3 are very consistent from year to year, though NH_3 concentrations are lower in 2019, possibly due to the CrIS data gap between March and June. There is good qualitative agreement with the in situ data, with the exception of the Wendell site, which was discussed above. Moreover, the hotspots are very well correlated with the areas of high dairy density (Figure 11, upper right). These maps illustrate the power of the CrIS data to provide context to in situ measurements and far more information on the spatial

variability in NH_3 than is normally available from emissions databases in the United States, which are frequently at county level. Data from these gridded maps could be used to constrain emission inventories over much larger areas and at more frequent intervals than is currently possible. This oversampling analysis demonstrates the utility of providing users with Level 2 products, since they then choose the sampling periods and resolution that are most appropriate for their purposes and are best suited to the times and regions under investigation. For example, a user might want to study the variability of NH_3 over just the urban area of Mexico City (e.g. Herrera et al., 2022). Level 3 products provide no such flexibility.

6.0 Conclusions and future work

The comparison between the DISCOVER-AQ aircraft datasets and the co-located AIRS and CrIS data provide useful information for end-users who would like to use CrIS and AIRS data over strong source regions. Given the large uncertainties in the aircraft data above the MLH, the profiles can only be evaluated within the mixed layer. Average biases in this layer, after smoothing errors are accounted for, are below or close to 1 ppbv. The AIRS and CrIS profiles individually have large estimated uncertainties, ranging from 5 to 50%. On average in California, as the error analysis in Figure 6a and 6b indicate, the a posteriori estimated error underestimates the actual uncertainties, probably due to the thermal inversions and high sub-pixel variability, which is expected, since these two factors are not accounted for in the error estimate. Ongoing work is attempting to quantity the effect of sub-pixel variability by analyzing data from multiple aircraft passes over the same CrIS pixel; these data were obtained during the TRANSAM (http://catalog.eol.ucar.edu/trans2am) campaign in 2022. Further data from the HYTES (https://hytes.jpl.nasa.gov/) instrument flown over the Imperial Valley is also being evaluated.

Over Colorado the estimated uncertainty is very close to measured uncertainty within the mixed layer, suggesting the error sources are properly accounted for in this region.

This study has not attempted to untangle the impact of the errors in the retrieved water vapor from those of temperature on the NH_3 errors. Such an analysis is an important and ongoing task, as global maps of CrIS NH3 have revealed artificial hotspots of NH_3 over tropical oceans, where humidity is high. There is a weak water vapor line in the spectral region used in the NH3 retrievals, which is possibly leading to these artifacts.

The column data analysis suggests that either there is non-neglible NH_3 above the top of the aircraft profile, or the retrievals are overestimating NH_3 above this altitude, because the a priori profile shape is very different from the true profile shape. More measurements and more accurate of NH_3 in this altitude region, along with experimenting a priori profile shapes with longer tails and a faster vertical decay, are required to resolve this issue.

The Magic Valley analysis clearly demonstrates the importance of having more than a few dozen data point measurements to obtain useful information from space-based retrievals of NH_3. With 464 observations over three years, over a limited region, it was possible to obtain a clear picture of the source distribution in the Magic Valley through the application of a physics based oversampling algorithm. Further work will apply this approach to other regions and times and use the resulting maps to estimate emissions and to improve reactive nitrogen deposition estimates.

Acknowledgements:

Part of this research was carried out at the Jet Propulsion Laboratory (JPL), California Institute of Technology, under a contract with NASA. Susan Kulawik made substantial contributions to the development of the MUSES algorithms and software at JPL.

This research has been supported by NASA via the TRopospheric Ozone and its Precursors from Earth System Sounding (TROPESS) project at JPL and by a Suomi National Polar-Orbiting Partnership (NPP) and the Joint Polar Satellite System (JPSS) Satellites Standard Products for Earth System Data Records grant (80NSSC21K1963) to Karen Cady-Pereira at AER.

This research was also supported, in part, by the U.S. Department of Agriculture, Agricultural Research Service. Mention of trade names or commercial products in this publication is solely for the purpose of providing specific information and does not imply recommendation or endorsement by the U.S. Department of Agriculture. USDA is an equal opportunity provider and employer.

NH_3 measurements during DISCOVER-AQ were supported by the Austrian Federal Ministry for Transport, Innovation and Technology (bmvit) through the Austrian Space Applications Programme (ASAP) of the Austrian Research Promotion Agency (FFG) (grants #833451, #840086). Tomas Mikoviny is acknowledged for field support; Ionicon Analytik is acknowledged for instrumental support.

Kang Sun acknowledges support from NASA ACMAP (80NSSC19K0988).

Data availability

MUSES AIRS and CrIS NH_3 products from S-NPP are available via the GES-DISC from the NASA Tropospheric Ozone and Precursors from Earth System Sounding (TROPESS) project at https://disc.gsfc.nasa.gov/datasets/TRPSDL2NH3AIRSFS_1/summary?keywords=tropess%20nh3, (Bowman, 2021a) and https://disc.gsfc.nasa.gov/datasets/TRPSDL2NH3CRSFS_1/summary?keywords=tropess%20nh3, (Bowman 2021b) respectively. The AIRS and CrIS datasets matched with aircraft used here for validation are available from the authors on request.

Author contributions

KCP designed the project, carried out the MUSES retrievals, created the preliminary plots, analyzed the results and wrote the manuscript. XG, RW and MZ provided the co-located aircraft data and made suggestions for the manuscript. AL provided the Magic Valley data and

contributed relevant text. KS provided the oversampling code and revised the manuscript. VP and MS provided useful insights and revised the manuscript. CC and EB created all the plots. MM and AW obtained the DISCOVER-AQ data. VK designed and built the MUSES software.

References

Aneja, V. P., Nelson, D. R., Roelle, P. A., Walker, J. T., and Battye, W.: Agricultural ammonia emissions and ammonium concentrations associated with aerosols and precipitation in the southeast United States, J. Geophys. Res., 108(D4), 4152, https://doi.org/10.1029/2002JD002271, 2003.

Aumann, H. H., Chahine, M. T., Goldberg, M. D., Kalnay, E., McMillin, L. M., Revercomb, H., Rosenkranz, P. W., Smith, W. L., Staelin, D. H., Strow, L. L., and Suskind, J.: AIRS/AMSU/HSB on the Aqua mission: Design, science objectives, data products and processing systems, IEEE T. Geosci. Remote, 41, 253–264, 2003.

Battye, W., Aneja, V. P., and Schlesinger, W. H.: Is nitrogen the next carbon? Earth's Future, 5(9), 894–904, 2017.

Beer, R., Shephard, M. W., Kulawik, S. S., Clough, S. A., Eldering, A., Bowman, K. W., Sander, S. P., Fisher, B. M., Payne, V. H., Luo, M., Osterman, G. B., and Worden, J. R.: First satellite observations of lower tropospheric ammonia and methanol, Geophys. Res. Lett., 35, L09801, https://doi.org/10.1029/2008GL033642, 2008.

Behera, S. N., Sharma, M., Aneja, V. P., and Balasubramanian, R.: Ammonia in the atmosphere: A review on emission sources, atmospheric chemistry and deposition on terrestrial bodies, Environ. Sci. Pollut. R., 20(11), 8092–8131, https://doi.org/10.1007/s11356-013-2051-9, 2013.

Berkhout, A. J. C., Swart, D. P. J., Volten, H., Gast, L. F. L., Haaima, M., Verboom, H., Stefess, G., Hafkenscheid, T., and Hoogerbrugge, R.: Replacing the AMOR with the miniDOAS in the ammonia monitoring network in the Netherlands, Atmos. Meas. Tech., 10, 4099–4120, https://doi.org/10.5194/amt-10-4099-2017, 2017.

Bowman, K. W., Rodgers, C. D., Kulawik, S. S., Worden, J., Sarkissian, E., Osterman, G., Steck, T., Lou, M., Eldering, A., and Shephard, M.: Tropospheric emission spectrometer: Retrieval method and error analysis, IEEE T. Geosci. Remote, 44(5), 1297–1307, 2006.

Bowman , K.W., TROPESS AIRS-Aqua L2 Ammonia for Forward Stream, Standard Product V1, Greebelt, MD, USA, Goddard Earth Sciences Data and Information Services Center (GES DISC), 10.5067/EYXLPVGTSWFF, 2021a.

Bowman, K.W.,(TROPESS CrIS-SNPP L2 Ammonia for Forward Stream, Standard Product V1, Greenelt, MD, USA, Goddard Earth Sciences Data and Information Services Center (GES DISC), 10.5067/B4TF7ND8A3O7, 2021b.

Cao, H., Henze, D. K., Cady-Pereira, K., McDonald, B. C., Harkins, C., Sun, K., Bowman, K. W., Fu, T.-M. and Nawaz, M. O.: COVID-19 lockdowns afford the first satellite-based confirmation that vehicles are an under-recognized source of urban NH_3 pollution in Los Angeles, Environ. Sci. Tech. Let., 9(1), 3–9, https://doi.org/10.1021/acs.estlett.1c00730, 2022.

Cohen, A. J., Aaron, J., Brauer, M., Burnett, R., Anderson, H. R., Frostad, J., Estep, K., Balakrishnan, K., Brunekreef, B., Dandona, L., Dandona, R., Feigin, V., Freedman, G., Hubbell, B., Jobling, A., Kan, H., Knibbs, L., Liu, Y., Martin, R., Morawska, L., Pope, C. A., Shin, H., Straif, K., Shaddick, G., Thomas, M., van Dingenen, R., van Donkelaar, A., Vos, T., Murray, C., Forouzanfar, J. L., Mohammad, H.: Estimates and 25-year trends of the global burden of disease attributable to ambient air pollution: an analysis of data from the Global Burden of Diseases Study 2015, The Lancet, 389 (10082), 1907–1918, 2017.

Coheur, P. F., Clarisse, L., Turquety, S., Hurtmans, D., and Clerbaux, C.: IASI measurements of reactive trace species in biomass burning plumes, Atmos. Chem. Phys., 9(15), 5655–5667, https://doi.org/10.5194/acp-9-5655-2009, 2009.

Crawford, J. H., and Pickering, K. E.: DISCOVER-AQ: Advancing strategies for air quality observations in the next decade, EM Magazine, Air & Waste Management Association, 9, 4–7. Retrieved from https://www.awma.org/content.asp?admin=Y&contentid=301, 2014.

Dammers, E., Shephard, M. W., Palm, M., Cady-Pereira, K., Capps, S., Lutsch, E., Strong, K., Hannigan, J. W., Ortega, I., Toon, G. C., Stremme, W., Grutter, M., Jones, N., Smale, D., Siemons, J., Hrpcek, K., Tremblay, D., Schaap, M., Notholt, J., and Erisman, J. W.: Validation of the CrIS fast physical NH_3 retrieval with ground-based FTIR, Atmos. Meas. Tech., 10, 2645–2667, https://doi.org/10.5194/amt-10-2645-2017, 2017.

Dammers, E., McLinden, C. A., Griffin, D., Shephard, M. W., Van Der Graaf, S., Lutsch, E., Schaap, M., Gainairu-Matz, Y., Fioletov, V., Van Damme, M., Whitburn, S., Clarisse, L., Cady-Pereira, K., Clerbaux, C., Coheur, P. F., and Erisman, J. W.: NH_3 emissions from large point sources derived from CrIS and IASI satellite observations, Atmos. Chem. Phys., 19, 12261–12293, https://doi.org/10.5194/acp-19-12261-2019, 2019.

Emission Database for Global Atmospheric Research (EDGAR), release version 4.3.1, http://edgar.jrc.ec.europa.eu/overview.php?v=431 (2016).

Erisman, J. W., Sutton, M. A., Galloway, J., Klimont, Z., and Winiwarter, W.: How a century of ammonia synthesis changed the world? Nat. Geosci., 1(10), 636–639, https://doi.org/10.1038/ngeo325, 2008.

Fu, D., Worden, J. R., Liu, X., Kulawik, S. S., Bowman, K. W., and Natraj, V.: Characterization of ozone profiles derived from Aura TES and OMI radiances, Atmos. Chem. Phys., 13(6), 3445–3462, https://doi.org/10.5194/acp-13-3445-2013, 2013.

Fu, D., Bowman, K. W., Worden, H. M., Natraj, V., Worden, J. R., Yu, S., Veefkind, P., Aben, I., Landgraf, J., Strow, L., and Han, Y.: High-resolution tropospheric carbon monoxide profiles retrieved from CrIS and TROPOMI, Atmos. Meas. Tech., 9, 2567–2579, https://doi.org/10.5194/amt-9-2567-2016, 2016.

Fu, D., Kulawik, S. S., Miyazaki, K., Bowman, K. W., Worden, J. R., Eldering, A., Livesey, N. J., Teixeira, J., Irion, F. W., Herman, R. L., Osterman, G. B., Liu, X., Levelt, P. F., Thompson, A. M., and Luo, M.: Retrievals of tropospheric ozone profiles from the synergism of AIRS and OMI: methodology and validation, Atmos. Meas. Tech., 11(10), 5587–5605, https://doi.org/10.5194/amt-11-5587-2018-supplement, 2018.

Guo, X., Wang, R., Pan, D., Zondlo, M.A., Clarisse, L., Van Damme, M., Whitburn, S., Coheur, P.-F., Clerbaux, C., Franco, B., Golston, L. M., Wendt, L., Sun, K., Tao, L., Miller, D.,

Mikoviny, T., Muller, M., Wisthaler, A., Tevlin, A. G., Murphy, J. G., Nowak, J. B., Roscioli, J. R., Vokamer, R., Kille, N., Neuman, J. A., Eilerman, S. J., Crawford, J. H., Yacovitch, T. A., Barrick, J. D., Scarino, A. J.: Validation of IASI satellite ammonia observations at the pixel scale using in situ vertical profiles, J. Geophys. Res.-Atmos.,126, e2020JD033475, https://doi.org/10.1029/2020JD033475, 2021.

Hegarty, J. D., Cady-Pereira, K. E., Payne, V. H., Kulawik, S. S., Worden, J. R., Kantchev, V., Worden, H. M., McKain, K., Pittman, J. V., Commane, R., Daube Jr., B. C., and Kort, E. A.: Validation and error estimation of AIRS MUSES CO profiles with HIPPO, ATom, and NOAA GML aircraft observations, Atmos. Meas. Tech., 15, 205–223, https://doi.org/10.5194/amt-15-205-2022, 2022.

Herrera, B., Bezanilla, A., Blumenstock, T., Dammers, E., Hase, F., Clarisse, L., Magaldi, A., Rivera, C., Stremme, W., Strong, K., Viatte, C., Van Damme, M., and Grutter, M.: Measurement report: Evolution and distribution of NH_3 over Mexico City from ground-based and satellite infrared spectroscopic measurements, Atmos. Chem. Phys., 22, 14119–14132, https://doi.org/10.5194/acp-22-14119-2022, 2022.

Höpfner, M., Ungermann, J., Borrmann, S., Wagner, R., Spang, R., Riese, M., Stiller, G., Appel, O., Batenburg, A., Bucci, S., Cairo, F., Dragoneas, A., Friedl-Vallon, F., Hünig, A., Johansson, S., Krasaukas, L., Legras, B., Leisner, T., Mahnke, C., Möhler, O., Molleker, S., Müller, R., Neubert, T., Orphal, J., Preusse, P., Rex, M., Saathoff, H., Stroh, F., Weigel, R., and Wohltmann, I.: Ammonium nitrate particles formed in upper troposphere from ground ammonia sources during Asian monsoons, Nat. Geosci., 12(8), 608–612, https://doi.org/10.1038/s41561-019-0385-8, 2019.

Kille, N., Chiu, R., Frey, M., Hase, F., Sha, M. K., Blumenstock, T., et al. (2019). Separation of methane emissions from agricultural and natural gas sources in the Colorado Front Range. Geophysical Research Letters, 46(7), 3990–3998. https://doi.org/10.1029/2019GL082132

Kulawik, S. S., Worden, J., Eldering, A., et al., Implementation of cloud retrievals for Tropospheric Emission Spectrometer (TES) atmospheric retrievals: 1. Description and characterization of errors on trace gas retrievals, *J. Geophys. Res., 111,* D24204, doi:10.1029/2005JD006733~~, 2006.~~

Lelieveld, J.; Evans, J. S.; Fnais, M.; Giannadaki, D.; Pozzer, A. The contribution of outdoor air pollution sources to premature mortality on a global scale. Nature, 525, 367−371, 2015.

Leytem, A. B., Dungan, R. S., Bjorneberg, D. L., and Koehn, A. C.: Emissions of ammonia, methane, carbon dioxide, and nitrous oxide from dairy cattle housing and manure management systems, J. Environ. Qual., 40:1383–1394, 2011.

Leytem, A. B., Dungan, R. S., Bjorneberg, D. L., and Koehn, A. C.: Greenhouse gas and ammonia emissions from an open-freestall dairy in southern Idaho, J. Environ. Qual., 42:10–20, 2013.

Leytem, A. B., Williams, P., Zuidema, S., Martinez, A., Chong, Y. L., Vincent, A., Vincent, A., Cronan, D., Kliskey, A., Wulfhorst, J. D., Alessa, L., and Bjorneberg, D.: Cycling phosphorus and nitrogen through cropping systems in an intensive dairy production region, Agronomy. 11, 1005, https://doi.org/10.3390/agronomy11051005, 2021.

Liu, Z., Zhou, M., Chen, Y., Chen, D., Pan, Y., Song, T., Ji, D., Chen, Q., and Zhang, L.: The nonlinear response of fine particulate matter pollution to ammonia emission reductions in

North China, Environ. Res. Lett.,16, 034014, https://doi.org/10.1088/1748-9326/abdf86, 2021.

Marais, E. A., Pandey, A. K., Van Damme, M., Clarisse, L., Coheur, P.-F.,Shephard, M. W., et al.. UK ammonia emissions estimated withsatellite observations and GEOS-Chem. Journal of Geophysical Research:Atmospheres, 126, e2021JD03523 https://doi.org/10.1029/2021JD035237, 2021.

Miller, D. J., K. Sun, L. Tao, M. A. Khan, and M. A. Zondlo (2014), Open-path, quantum cascade-laser-based sensor for high-resolution atmospheric ammonia measurements, Atmos. Meas. Tech., 7, 81–93, doi:10.5194/amt-7-81-2014.Müller, M., Mikoviny, T., Feil, S., Haidacher, S., Hanel, G., Hartungen, E., et al.: A compact PTR-ToF-MS instrument for airborne measurements of volatile organic compoundsat high spatiotemporal resolution,Atmospheric Measurement Techniques, 7(11), 3763–3772. https://doi.org/10.5194/amt-7-3763-2014, 2014.

Nowak, J. B., Neuman, J. A., Bahreini, R., Brock, C. A., Middlebrook, A. M., Wollny, A. G., Holloway, J. S., Peischl, J., Ryerson, T. B., Fehsenfeld, F. C.: Airborne observations of ammonia and ammonium nitrate formation over Houston, Texas, J. Geophys. Res., 115(22), D22304, https://doi.org/10.1029/2010JD014195, 2010.

Nowak, J. B., Neuman, J. A., Bahreini, R., Middlebrook, A. M., Holloway, J. S., McKeen, S. A.: Ammonia sources in the California South Coast Air Basin and their impact on ammonium nitrate formation, Geophys. Res. Lett., 39(7), 2012.

Paulot, F., and Jacob, D. J: Hidden cost of US agricultural exports: particulate matter from ammonia emissions, Environ. Sci.Tech., 48 (2), 903–908, 2014.

Paulot, F., Jacob, D. J., and Henze, D. K.: Sources and processes contributing to nitrogen deposition: an adjoint model analysis applied to biodiversity hotspots worldwide, Environ. Sci.Tech., 47(7), 3226–3233, 2013.

Pinder, R. W., J. T. Walker, J. O. Bash, K. E. Cady-Pereira, D. K. Henze, M. Luo, G.B.Osterman, and M. W. Shephard: Quantifying spatial and seasonal variability in atmospheric ammonia with in situ and space-based observations, Geophys. Res. Lett., 38, L04802, doi:10.1029/2010GL046146, 2011.

Pollack, I. B., Lindaas, J., Roscioli, J. R., Agnese, M., Permar, W., Hu, L., and Fischer, E. V.: Evaluation of ambient ammonia measurements from a research aircraft using a closed-path QC-TILDAS operated with active continuous passivation, Atmos. Meas. Tech., 12, 3717–3742, https://doi.org/10.5194/amt-12-3717-2019, 2019.

Puchalski, M.A., Rogers, C.M., Baumgardner, R., Mishoe, K.P., Price, G., Smith, M.J., Watkins, N., and Lehmann, C.M.: A statistical comparison of active and passive ammonia measurements collected at Clean Air Status and Trends Network (CASTNET) sites, Environmental Science: Processes & Impacts, 17, 358-369, http://dx.doi.org/10.1039/C4EM00531G, 2015.

Pope, C., III; Ezzati, M.; Dockery, D. W.: Fine-particulate air pollution and life expectancy in the United States, N. Engl. J. Med., 360, 376−386, 2009.

Rodgers, C. D.: Inverse Methods for Atmospheric Sounding, Theory and Practice, World Scientific Publishing, London, 2000.

Rodgers, C. D., and Connor, B. J.: Intercomparison of remote sounding instruments, J. Geophys. Res., 108, 4116, https://doi.org/10.1029/2002jd002299, 2003.

Roscioli, J. R., Zahniser, M. S., Nelson, D. D., Herndon, S. C., and Kolb, C. E.: New approaches to measuring sticky molecules: improvement of instrumental response times using active passivation, J. Phys. Chem. A, 120, 1347–1357, https://doi.org/10.1021/acs.jpca.5b04395, 2016.

Shephard, M. W., Cady-Pereira, K. E., Luo, M., Henze, D. K., Pinder, R. W., Walker, J. T., Rinsland, C. P., Bash, J. O., Zhu, L., Payne, V., and Clarisse, L.: TES ammonia retrieval strategy and global observations of the spatial and seasonal variability of ammonia, Atmos. Chem. Phys., 11, 10743–10763, https://doi.org/10.5194/acp-11-10743-2011, 2011.

Shephard, M. W., McLinden, C. A., Cady-Pereira, K. E., Luo, M., Moussa, S. G., Leithead, A., Liggio, J., Staebler, R. M., Akingunola, A., Makar, P., Lehr, P., Zhang, J., Henze, D. K., Millet, D. B., Bash, J. O., Zhu, L., Wells, K. C., Capps, S. L., Chaliyakunnel, S., Gordon, M., Hayden, K., Brook, J. R., Wolde, M., and Li, S.-M.: Tropospheric Emission Spectrometer (TES) satellite observations of ammonia, methanol, formic acid, and carbon monoxide over the Canadian oil sands: validation and model evaluation, Atmos. Meas. Tech., 8, 5189–5211, https://doi.org/10.5194/amt-8-5189-2015, 2015.

Shephard, M. W., and Cady-Pereira, K. E.: Cross-track Infrared Sounder (CrIS) satellite observations of tropospheric ammonia, Atmos. Meas. Tech., 8, 1323–1336, https://doi.org/10.5194/amt-8-1323-2015, 2015.

Shephard, M. W., Dammers, E., Cady-Pereira, K. E., Kharol, S. K., Thompson, J., Gainariu-Matz, Y., Zhang, J., McLinden, C. A., Kovachik, A., Moran, M. and Bittman, S.: Ammonia measurements from space with the Cross-track Infrared Sounder: characteristics and applications., Atmos. Chem.Phys. 20(4), 2277–2302, 2020.

Skjøth, C. A., and Geels, C.: The effect of climate and climate change on ammonia emissions in Europe, Atmos. Chem. Phys., 13, 117–128, https://doi.org/10.5194/acp-13-117-2013, 2013.

Sun, K., Cady-Pereira, K. E., Miller, D. J., Tao, L., Zondlo, M. A., Nowak, J. B., Neuman, A., Mikoviny, T., Mueller, M., Wisthaler, A., Scarino, A. J., and Hostetler, C. A.: Validation of TES ammonia observations at the single pixel scale in the San Joaquin Valley during DISCOVER-AQ, J. Geophys. Res.-Atmos., 120, https://doi.org/10.1002/2014JD022846, 2015.

Sun, K., Tao, L., Miller, D. J., Pan, D., Golston, L. M., Zondlo, M. A., Griffin, R. J., Wallace, H. W., Leong, Y. J., Yang, M. M., Zhang, Y., Mauzerall, D. L., Zhu, T.: Vehicle emissions as an important urban ammonia source in the United States and China, Environ. Sci. Tech., 51(4), 2472–2481, https://doi.org/10.1021/acs.est.6b02805, 2017.

Sun, K., Zhu, L., Cady-Pereira, K., Chan Miller, C., Chance, K., Clarisse, L., Coheur, P.-F., González Abad, G., Huang, G., Liu, X., Van Damme, M., Yang, K., and Zondlo, M.: A physics-based approach to oversample multi-satellite, multispecies observations to a common grid, Atmos. Meas. Tech., 11, 6679–6701, https://doi.org/10.5194/amt-11-6679-2018, 2018.

Susskind, J., Barnet, C. D., and Blaisdell, J. M.: Retrieval of atmospheric and surface parameters from AIRS/AMSU/HSB data in the presence of clouds, IEEE T. Geosci. Remote, 41, 390–409, 2003.

Tournadre, B., Chelin, P., Ray, M., Cuesta, J., Kutzner, R. D., Landsheere, X., Fortems-Cheiney, A., Flaud, J.-M., Hase, F., Blumenstock, T., Orphal, J., Viatte, C., and Camy-Peyret, C.: Atmospheric ammonia (NH_3) over the Paris megacity: 9 years of total column observations from ground-based infrared remote sensing, Atmos. Meas. Tech., 13, 3923–3937, https://doi.org/10.5194/amt-13-3923-2020, 2020.

Sutton, M. A., Reis, S., Riddick, S. N., Dragosits, U., Nemitz, E., Theobald, M. R., Tang, Y. S., Braban, C. F., Vieno, M., Dore, A. J., Mitchell, R. F., Wanless, S., Daunt, F., Fowler, D., Blackall, T. D., Milford, C., Flechard, C. R., Loubet, B., Massad, R., Cellier, P., Personne, E., Coheur, P. F., Clarisse, L., Van Damme, M., Ngadi, Y., Clerbaux, C., Skjøth, C. A., Geels, C., Hertel, O., Wichink Kruit, R. J., Pinder, R. W., Bash, J. O., Walker, J. T., Simpson, D., Horváth, L., Misselbrook, T. H., Bleeker, A., Dentener, F., and de Vries, W.: Towards a climate-dependent paradigm of ammonia emission and deposition, Philos. Trans. R. Soc. Lond. B. Biol. Sci., 368(1621), 20130166, https://doi.org/10.1098/rstb.2013.0166, 2013.

Van Damme, M., Erisman, J. W., Clarisse, L., Dammers, E., Whitburn, S., Clerbaux, C., Dolman, A. J., and Coheur, P. F.: Worldwide spatiotemporal atmospheric ammonia (NH_3) columns variability revealed by satellite, Geophys. Res. Lett., 42(20), 8660–8668, https://doi.org/10.1002/2015GL065496, 2015a.

Van Damme, M., Clarisse, L., Dammers, E., Liu, X., Nowak, J. B., Clerbaux, C., Flechard, C. R., Galy-Lacaux, C., Xu, W., Neuman, J. A., Tang, Y. S., Sutton, M. A., Erisman, J. W., and Coheur, P. F.: Towards validation of ammonia (NH_3) measurements from the IASI satellite, Atmos. Meas. Tech., 8, 1575–1591, https://doi.org/10.5194/amt-8-1575-2015, 2015b.

Van Damme, M., Clarisse, L., Whitburn, S., Hadji-Lazaro, J., Hurtmans, D., Clerbaux, C., Coheur P.: Industrial and agricultural ammonia point sources exposed, Nature, 564, 99–103, https://doi.org/10.1038/s41586-018-0747-1, 2018.

von Bobrutzki, K., Braban, C. F., Famulari, D., Jones, S. K., Blackall, T., Smith, T. E. L., Blom, M., Coe, H., Gallagher, M., Ghalaieny, M., McGillen, M. R., Percival, C. J., Whitehead, J. D., Ellis, R., Murphy, J., Mohacsi, A., Pogany, A., Junninen, H., Rantanen, S., Sutton, M. A., and Nemitz, E.: Field inter-comparison of eleven atmospheric ammonia measurement techniques, Atmos. Meas. Tech., 3, 91–112, https://doi.org/10.5194/amt-3-91-2010, 2010.

Wang, R., Guo, X., Pan, D., Kelly, J. T., Bash, J. O., Sun, K., et al., Monthly patterns of ammonia over the contiguous United States at 2-km resolution. *Geophysical Research Letters*, 48, e2020GL090579. https://doi.org/10.1029/2020GL090579, 2021.

Warner, J. X., Wei, Z., Strow, L. L., Dickerson, R. R., and Nowak, J. B.: The global tropospheric ammonia distribution as seen in the 13-year AIRS measurement record, Atmos. Chem. Phys., 16, 5467–5479, https://doi.org/10.5194/acp-16-5467-2016, 2016.

Warner, J. X., Dickerson, R. W., Wei, Z., Strow, L. L., Wang, Y., and Liang, Q.: Increased atmospheric ammonia over the world's major agricultural areas detected from space, Geophys. Res. Lett., 44, https://doi.org/10.1002/2016GL072305, 2017.

Whitburn, S., Van Damme, M., Kaiser, J. W., van der Werf, G. R., Turquety, S., Hurtmans, D, Clarisse, L., Clerbaux, C., and Coheur, P. F.: Ammonia emissions in tropical biomass burning regions: Comparison between satellite-derived emissions and bottom up _re inventories, Atmos. Environ., 121, 42–854, 2015.

Whitburn, S., Van Damme, M., Clarisse, L., Turquety, S., Clerbaux, C., and Coheur, P.-F.:

Doubling of annual ammonia emissions from the peat fires in Indonesia during the 2015 El Niño, Geophys. Res. Lett., 43, 2016GL070,620, 2016.

Worden, J., Bowman, K., Noone, D., Beer, R., Clough, S., Eldering, A., Fisher, B., Goldman, A., Gunson, M., Herman, R., Kulawik, S., Lampel, M., Luo, M., Osterman, G., Rinsland, C., Rodgers, C., Sander, S., Shephard, M., and Worden, H.: Tropospheric Emission Spectrometer observations of the tropospheric HDO/H2O ratio: Estimation approach and characterization, J. Geophys. Res., 111, D16309, https://doi.org/10.1029/2005JD006606, 2006.

Xu, P., Liao, Y. J., Lin, Y. H., Zhao, C. X., Yan, C. H., Cao, M. N., Wang, G. S., and Luan, S. J.: High-resolution inventory of ammonia emissions from agricultural fertilizer in China from 1978 to 2008, Atmos. Chem. Phys., 16, 1207–1218, https://doi.org/10.5194/acp-16-1207-2016, 2016.

Zavyalov, V., Esplin, D., Scott., D., Esplin, B., Bingham, G., Hoffman, E., Lietzke, C., Predina, J., Frain, R., Suwinski, L., Han, Y., Major, C., Graham, B., Phillips, L.: Noise performance of the CrIS instrument, J. Geophys. Res.-Atmos., 118, 13,108–13,120, https://doi.org/10.1002/2013JD020457, 2013.

Zhu, L., Henze, D. K., Cady-Pereira, K. E., Shephard, M. W., Luo, M., Pinder, R. W., Bash, J. O., and Jeong, G.-R.: Constraining U.S. ammonia emissions using TES remote sensing observations and the GEOS-Chem adjoint model, J. Geophys. Res.-Atmos., 118, https://doi.org/10.1002/jgrd.50166, 2013.